LA-UR-20-27504
Approved for public release; distribution is unlimited.

Title: First Examination of Irradiated Fuel with Pulsed Neutrons at LANSCE – Preliminary Results

Author(s): Vogel, Sven C.
Balke, Thilo
Bouman, Charles A.
Capriotti, Luca
Harp, Jason M.
Long, Alexander Makenzie
Schaper, Danielle
Tremsin, Anton S.
Wohlberg, Brendt Egon

Intended for: Report

Issued: 2020-09-23

First Examination of Irradiated Fuel with Pulsed Neutrons at LANSCE – Preliminary Results

Nuclear Technology Research and Development

Prepared for
U.S. Department of Energy
Nuclear Technology Research and Development Program
Advanced Fuels Campaign

Sven C. Vogel[1], Thilo Balke[1,2], Charles A. Bouman[2], Luca Capriotti[3], Jason M. Harp[4], Alex M. Long[1], Danielle C. Schaper[1], Anton S. Tremsin[5], Brendt E. Wohlberg[1]
[1]LANL, [2]Purdue University, [3]INL, [4]ORNL, [5]UC Berkeley,

September 18, 2020

LA-UR-20-XXXXX **M3FT-20LA020201023**

SUMMARY

We present preliminary results on the characterization of an irradiated U-10Zr-1Pd fuel sample that was prepared from the irradiated AFC-3A-R5A sample. U-10Zr metallic fuels are researched as host materials for potential transmutation fuels and the addition of palladium strives to bind lanthanides, thus preventing fuel-cladding chemical interactions (FCCI). These interactions limit the lifetime of metallic fuels and are caused by migration of lanthanide fission products to the periphery of the fuel slug, where they start to interact with the D9 or HT9 steel cladding, ultimately leading to failure of the mechanical integrity of the cladding.

Neutrons offer bulk characterization of irradiated materials for which X-ray tomography methods are not suitable due to the immense gamma background emitted from the samples. In particular pulsed neutrons provide information from the ability to resolve the neutron energy using their time-of-flight and thus the potential to utilize neutron absorption resonance to characterize the spatial distribution of isotopes. This, in turn, may allow to characterize the distribution of fission and neutron capture products non-destructively and may ultimately be applied to the bulk of an irradiation capsule prior to destructive post-irradiation examination to identify regions of interest. To allow the characterization of entire irradiation capsules, a cask is under development in the advanced post-irradiation work package at LANL and progress on this development was reported elsewhere. In parallel, an irradiated U-10Zr-1Pd sample cut from the AFC-3A-R5A irradiation was shipped to LANL and will be fully characterized with an NSUF funded rapid turnaround experiment (RTE) in the 2020 LANSCE run cycle. The sample emits at a dose rate of ~3R/hr on contact and is therefore manageable with remote handling, without requiring a cask. The disk-shaped material is larger than samples prepared for analysis using electron or X-ray methods and is therefore an intermediate step towards characterization of bulk samples at LANSCE. However, since it covers the full diameter of the irradiated fuel slug, some insight on redistribution of elements, spatially resolved information on microstructure, e.g. phase composition and texture, will be possible using the pulsed neutron-based methods developed for fuel characterization at LANSCE.

This report describes the development of procedures to handle the sample at LANSCE as well as preliminary data and results from tests conducted in December 2019 on the energy-resolved neutron imaging (ERNI) beam line at flight path 5 and the high pressure-preferred orientation diffractometer (HIPPO) at LANSCE. This effort is a collaboration between LANL, INL, and ORNL. To compare our capabilities with prior work, we present an overview of previously reported bulk characterization of irradiated or spent fuels. The overview addresses neutron diffraction and neutron absorption resonance spectroscopy, both of which have only few reported applications on irradiated or spent nuclear fuel, as well as neutron radiography. This literature review was already described in a previous report but is repeated here to put our current efforts in context of previous work.

CONTENTS

FIGURES

TABLES

ACRONYMS

AECL	Atomic Energy of Canada Limited
APS	Advanced Photon Source
AFC	Advanced Fuel Campaign
ANDE	Advanced Non-destructive Examination
ATF	Accident Tolerant Fuel
ATR	Advanced Test Reactor
BRR	BEA Research Reactor
BWR	Boiling Water Reactor
CCD	Charge-Coupled Device
CEA	French Alternative Energies and Atomic Energy Commission
CT	Computed Tomography
DOE	Department of Energy
DOE/NE	Department of Energy/Nuclear Energy program
DOT	Department of Transportation
EBS	Ethylene bis-stearate
ENDF	Evaluated Nuclear Data File
EPMA	Electron Probe Microanalysis
ERNI	Energy-resolved Neutron Imaging
FCCI	Fuel Cladding Chemical Interaction
FCMI	Fuel Cladding Mechanical Interaction
FCRD	Fuel Cycle Research and Development
FOV	Field of View
FP5	Flight-path 5 (imaging beam line at LANSCE)
FR	Fast Reactor
HEU	Highly Enriched Uranium
HFEF	Hot Fuels Examination Facility
HI	High Intensity
HIPPO	High Pressure/Preferred Orientation neutron diffractometer
IAEA	International Atomic Energy Agency
ICP-MS	Inductively coupled plasma mass spectrometry
IMCL	Irradiated Materials Characterization Laboratory
INL	Idaho National Laboratory
JAEA	Japan Atomic Energy Agency

LANL	Los Alamos National Laboratory
LANSCE	Los Alamos Neutron Science Center
LEU	Low enriched uranium
Linac	Linear Accelerator
LWR	Light Water Reactor
MA	Minor Actinides
MAMOX	Minor Actinide bearing Mixed Oxide Fuels
MCP	Multi-channel plate
MOX	Mixed Oxide Fuels
NDE	Non-Destructive Examination
ND-PIE	Non-Destructive Post Irradiation Examination
NNDC	National Nuclear Data Center (at Brookhaven National Laboratory)
NPDF	Neutron Powder Diffractometer/Neutron Pair Distribution Function
NRC	Nuclear Regulatory Commission
NRC	National Research Council Canada
NRS	Neutron Resonance Spectroscopy
NRTA	Neutron Resonance Transmission Analysis
NSLS	National Synchrotron Light Source
ORNL	Oak Ridge National Laboratory
O/M	Oxygen-to-Metal ratio
PCMI	Pellet Cladding Mechanical Interaction
PIE	Post Irradiation Examination
pRAD	Proton Radiography
PSI	Paul Scherrer Institute
PWR	Pressurized Water Reactor
RaMHaM	Radioactive Material Handling Mechanism
RE	Rare Earth element
ROI	Region of Interest
SEM	Scanning Electron Microscopy
SMARTS	Spectrometer for Materials Research at Temperature and Stress
TFRE	Transmutation Fuel with Rare earth inclusions
TMRS	Target-Moderator-Reflector System
TEM	Transmission Electron Microscopy
TOF	Time-of-flight

TREAT	Transient Reactor Test
UC	University of California
UN	Uranium nitride
U-Si	Uranium silicide (unspecified stoichiometry)
US	United States
VTR	Versatile Test Reactor

FIRST EXAMINATION OF IRRADIATED FUEL WITH PULSED NEUTRONS AT LANSCE – PRELIMINARY RESULTS

1. Introduction

1.1 Science-based Approach to Nuclear Fuel Development

A key enabler for a "science based approach" for accelerated development and qualification of new, fuel forms, such as accident tolerant or transmutation nuclear fuels, is an early and efficient understanding of material behavior at multiple length scales. For new fuel formulations, there is a dearth of irradiation testing experience. When representative irradiation tests take years, it is important to extract the maximum insight possible from each test. Post irradiation examination (PIE) of fuels is mature and sophisticated but measurements in hot cells are expensive and typically examine small volumes of irradiated fuels relying on a limited amount of knowledge of the bulk characteristics of the specimen to select the volume examined destructively. This leaves the possibility that key failure inducing phenomena will not be observed because of limited PIE. For these reasons, there is value in techniques that can quickly and non-destructively characterize properties over volumes consistent with standard fuel geometries. Applying such methods pre- and post-irradiation unambiguously determines the changes induced by irradiation. Such techniques can inform models predicting the performance of material in the reactor on the initial condition of samples and complement, guide, and leverage destructive post irradiation examination. For example, three dimensional characterization of complete fuel pellets within cladding after irradiation could identify regions that are representative of average and atypical response with parameters not accessible by presently applied techniques such as visual inspection, thermal neutron radiography, or acoustic methods.

Typical in-pile irradiation tests of new fuel types last months or years [1]. Demands on PIE may also impose a delay of years before individual samples can be studied. The resulting levels of radioactivity even for rodlets containing just a handful of pellets or metallic fuels of less than a cm^3 in volume require hot cells and remote manipulators to perform destructive PIE. The complexity and cost of such operations limit the PIE possible, thus, there is a premium on knowing where to measure by identifying regions of interest by as many non-destructive characterizations as possible. This research is focused on developing techniques for non-destructive examination of the bulk volume of rodlets containing multiple pellets or metallic fuels of similar dimensions [2].

The first step in this project is to "benchmark" the initial condition of candidate materials before irradiation [3]. The second step will be to make comparable non-destructive measurements on irradiated rodlets prior to their destructive examination in INL hot cells. Neutron, proton and (synchrotron) X-ray radiography/tomography techniques all pose opportunities for this endeavor [3]. By virtue of their stand-off capability and ability to probe materials despite an intense gamma field, neutrons and protons both offer potential for study of highly radioactive materials. At Los Alamos National Laboratory, neutron based techniques are routinely used to evaluate microstructure, phase and composition [4] and protons are widely used for dynamic radiography [5] with fuel characterization also demonstrated [6].

The programmatic emphases for developing advanced non-destructive examination (ANDE) techniques applicable to irradiated materials are two-fold. First, it will be possible to evaluate fuel materials to guide the destructive post-irradiation examination towards regions of interest that are not obvious with conventional techniques. This will help develop the statistical insight necessary to complement modeling and simulation data. Adding ANDE insight to the standard optical, thermal neutron and gamma ray insights will help identify regions where destructive examination can be focused. This will increase the return from PIE since regions of atypical irradiation performance are more likely to be discovered. A second reason for

ANDE lies in the desire to generate data as soon as possible after removal of the test samples from the reactor. This is a key requirement in accelerating the development and time to licensing of new fuel forms. The philosophy is consistent with improving diagnostics to offer faster turnaround and getting "more out of less". Programmatically, the capabilities under development sets the stage for routine pre-irradiation fuel examinations and potentially for post-irradiation examinations of accident tolerant fuels (ATF) or transmutation fuels.

The techniques employed at LANSCE use the pulsed neutron source at the Lujan Center. They rely on co-location with the 800MeV proton accelerator [7]. However, advances in small-scale accelerators for neutron generation (by D-D fusion) or laser-driven pulsed neutron sources [8,9] pose interesting opportunities [10]. Although such small scale sources are not currently capable of neutron production for measurements of the type described here, technological advance is ongoing. It is possible that, in the next decade, a "small-scale" laser-driven pulsed neutron source with sufficient neutron production performance might become available to provide "pool side" implementation of the techniques described in this report.

1.2 Scope and Goals of this activity

While characterization of entire irradiation capsules is the ultimate goal of this activity, smaller volumes with manageable radioactivity not requiring a cask for handling is in important intermediate step. In the current work, preliminary characterization of a 6 mm diameter, 1.5 mm thick sample with pulsed neutron at LANSCE is described. While in previous reports [2,3,11,12,13] these pulsed neutron techniques were described in detail and applied to un-irradiated materials, application to irradiated materials promise the highest return. These methods probe the bulk of a material and are applicable to actual fuels rather than custom-made research samples and are based on energy-resolved neutron imaging (ERNI) and neutron diffraction.

Pre-existing inclusions, density, chemical and isotopic inhomogeneities and cracks as well as microstructural features such as phase composition, texture or residual stresses can affect fuel behavior in an irradiation environment. For science based development initiatives it is hoped that qualification of new fuel systems can be achieved by fusing science insight with insights from fewer irradiation tests than has been true in the past. However, the goal of accelerated insight from fewer tests places more emphasis on pre-characterizing the condition of test fuel samples prior to irradiation as well as the need for more thorough bulk characterization of the whole irradiated volume to guide destructive examination of irradiated materials. Since neutrons are non-destructive, capable of interrogating whole pellets and sensitive to the mesoscale characteristics being implemented in models, they are uniquely suited for the study of prototype nuclear fuels. Non-destructive 3D maps of cracks, density, isotopic and geometry variation can be measured using neutrons in pellets or slugs prior to irradiation. The potential exists for making the same measurements post irradiation, the focus of the present report. The ultimate goal is to accelerate the time to insight, development and qualification of new nuclear fuels.

This initiative is focused on the application of neutrons to draw non-destructive insight on fresh nuclear fuel prior to irradiation and in the future on irradiated fuel. Neutron imaging and scattering techniques easily examine volumes of up to several cubic centimeters, consistent with typical rod assemblies of ceramic fuel pellets. Neutron scattering lengths for high and low atomic number elements are often comparable and allow efficient study of systems consisting of heavy and light elements.

The application of protons [4] and synchrotron X-rays [14] are also under consideration for these studies (though not reported here). Protons, like neutrons, have mean free paths in nuclear materials that facilitate characterization of cubic centimeters of material. The interaction of protons with matter is governed by nuclear and Coulomb interactions. They lose energy in the matter because of Coulomb scattering from the atomic electrons, and scatter from the nuclei both because of the strong interaction and the Coulomb interaction with the proton. Proton radiography is performed by illuminating a target object with a beam of protons and focusing the transmitted protons onto a scintillator screen [5]. Magnetic lenses offer different

magnification options. Synchrotron X-rays in excess of 50 keV also have applicability to fresh nuclear fuels and have been used in the study of U-Mo fuel [14]. This established their merit for studies of smaller regions of interest than are typically examined in neutron measurements. In future a holistic suite of measurement tools might naturally use neutrons, protons and synchrotron X-rays. The former two are available at LANSCE, which is a Nuclear Science User Facility partner since 2017, providing access to these capabilities to researchers working in the DOE/NE mission space. Small yet powerful synchrotron sources, allowing e.g. diffraction with 80 keV X-rays at a flux about two-three orders of magnitude below state-of-the-art engineering diffraction beamlines at APS, have recently become commercially available [15], paving the way to enabling a unique suite of pool-side characterization tools that are at present only available at large scale user facilities.

At a pulsed neutron sources time of flight energy sorting allows examination of samples by setting the contrast on isotopes [16,17] or crystal structures [18,19]. Neutron radiography detector technology has been revolutionized by the use of micro-channel plates (MCPs) for radiographic applications and proved a catalyst for these studies. The micro-channels are doped with neutron absorbing materials such as boron. They currently offer a spatial resolution of 55 µm at count rates of 10^8 $cm^{-2}s^{-1}$. Spatial resolution of 15 µm has been demonstrated at lower count rates [20].

At a LANL/INL workshop held in December of 2012 [2] a plan was conceived to use the advanced non-destructive examination techniques including neutron and proton radiography available at LANL and INL for analysis of irradiated fuel rodlets from the AFC-2C/2D irradiation at the ATR in Idaho [1]. In the first phase a set of mock-up rodlets were examined containing pellets of depleted uranium dioxide (dUO_2) with defects similar to that seen in irradiated fuel rodlets [16]. After these first measurements over the last few years, measurements have demonstrated the applicability of neutrons, protons and synchrotron X-rays to a range of ceramic and metallic fuels [3,11,12,13,13,22], including the ability to measure fission gas pressures [17,21] and measurements to complement modeling [11]. Several terabytes of imaging and scattering data have been collected. The ability to observe cladding dimensions, cracks, phase and isotopic species nondestructively and in three dimensions has been demonstrated. Development in data analysis and instrumentation is ongoing. Besides oxide fuels, extensive characterizations of accident tolerant UN/U_3Si_5 composite fuels [15,22] and U-20Pu-10Zr transmutation fuels [16] were reported.

Tomographic analysis of typical fuel/clad geometries using only thermal neutrons can elucidate three dimensional heterogeneities in a few hours using thermal neutron tomography. Determination of isotopic species requires measurements of resonances in the epithermal range, where both decreased flux and detector efficiency increase count times, and measurements on typical clad/pellet geometries typically require a few days of beam time for between three and six pellets for a full 3D isotope density measurement while bulk averages of e.g. enrichment levels can be done in less than one hour at LANSCE. Diffraction characterization in slices through the sample provides valuable additional information at beam times of about 0.5 days. Although early work focused on UO_2, recent initiatives have focused on developing fuels with enhanced accident tolerance, increased burn-up and reduced waste.

This report describes the first characterization of an irradiated fuel at LANSCE. The radioactivity of the sample is manageable by remote handling and does not a cask such as the one developed in parallel to this effort for characterization of entire radiation capsules. To provide context for this activity, a literature review on previously reported characterizations of irradiated or spent fuels is presented. We describe the experimental facilities utilized and give a brief overview on the AFC-3A-R5A sample from which the specimen characterized was prepared. The sample was received in late November 2019 and some preliminary data were collected before the end of the 2019 LANSCE run cycle in December. Results on those are presented and the complete measurements will be conducted in the 2020 run cycle with the data collection supported by an NSUF grant for this team.

2. Neutron Characterizations of Irradiated Materials Reported in the Literature

Several neutron characterizations of cm^3 sized irradiated materials are reported in the literature. However, while efforts in neutron radiography of fuels are reported from all over the world including Norway [23], Switzerland [24], China [25], Pakistan [26], Iran [27], Korea [28], South Africa [29], and India [30], to the best of our knowledge only the effort at the Paul Scherrer Institute (PSI) in Switzerland, at the Halden reactor in Norway, and at INL resulted in several publications spanning several years and only the neutron radiography conducted at INL can be considered routine operation of a neutron radiography facility for irradiated fuels after the recent shutdown of the Halden reactor in Norway. Parker and Joyce [31] provide an excellent overview of neutron as well as other imaging modalities to image nuclear fuel.

Reports of bulk diffraction characterization, only possible with neutrons owing to the limited penetration depth of X-rays into uranium-based materials, are even sparser. Similarly, only few applications of neutron resonance absorption spectroscopy of irradiated or spent fuels were found in the literature. While there are many reports of characterizations of much smaller amounts (<1 mm^3) prepared from larger irradiated volumes, it is noteworthy that bulk characterizations, e.g. entire pellets or fuel elements, beyond neutron radiography or visual inspection is very limited. It is however this type of characterization that allows to identify the sub-volume within e.g. an entire irradiation capsule that provides the greatest insight and advancement of knowledge when it is prepared destructively. This underlines the gap identified by the effort presented here. The characterizations, grouped into applications of neutron diffraction, neutron resonance absorption analysis, and neutron radiography, are briefly reviewed below.

2.1 Neutron Diffraction

Birtcher et al. characterized U_3Si and U_3Si_2 powders, contained in double walled vanadium containers, which were incrementally irradiated by neutrons from a neutron spallation source utilizing 500 MeV protons hitting a uranium target [32-36]. After decay times of up to 100 days, the samples were characterized in the General Purpose Powder Diffractometer (GPPD) at the Intense Pulsed Neutron Source (IPNS, now de-commissioned). This instrument is similar to the HIPPO instrument at LANSCE described below. No further details on sample handling or dose rates emitted from the radioactive samples were provided. The neutron time-of-flight diffraction data was analyzed using the Rietveld method [37], similar to analysis described below for the HIPPO diffractometer. Parameters such as the volume fraction of crystalline material during the amorphization, lattice parameters and unit cell volumes provide a detailed picture of the crystallographic response of the material as a function of damage measured in displacements per atom (dpa). Figure 1 provides some examples, allowing for instance to track the amorphization as a function of radiation damage as well as changes in lattice parameters and unit cell volume, indicative of strains occurring in the material that may have implications on the mechanical integrity of a fuel pellet (a powder was used for the experiment).

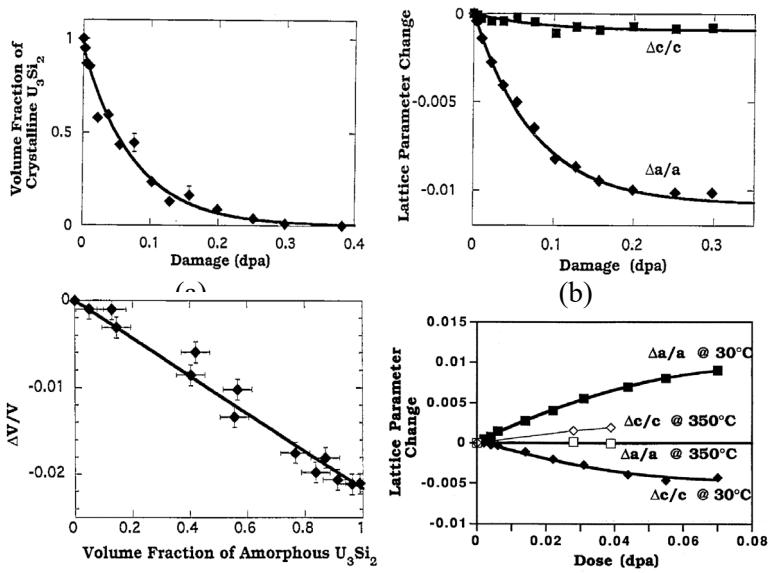

Figure 1: Results from Rietveld powder diffraction analysis of neutron irradiated U_3Si_2 from Birtcher et al.: (a) Volume fraction of crystalline U_3Si_2 as a function of damage; (b) relative lattice parameter changes of the tetragonal unit cell of U_3Si_2 as a function of damage; (c) correlation between unit cell changes as a function of volume fraction of the amorphous U_3Si_2 (all from [34]); (d) relative lattice parameter changes as a function of dose for irradiation at room temperature and at 350 ℃ (from [33]).

Conlon, Sears et al. report on neutron diffraction characterization of irradiated Al-U-7Mo fuels [38,39] as well as spent Al-U_3Si dispersion fuel from the Chalk River reactor [40]. For the latter, samples were taken from different locations of a spent fuel rod, correlating to different linear power, temperature (92-188°C) and burn-up conditions (63-90 atom % ^{235}U). Consistent with result from Birtcher et al. reported above, they found that no diffraction signal from U_3Si was present, indicating that the phase was entirely amorphous. For the Al-U-7Mo fuels irradiated to 60 atom% ^{235}U burnup, precipitation of several crystalline ternary phases such as (U,Mo)Al_2 and (U,Mo)Al_3 as well as small amounts of α-U and δ-U_2Mo were observed [39]. Figure 2 shows two shielding devices developed for this type of characterizations. Both were used at the reactor source at Chalk River and therefore are designed for *monochromatic* neutron powder diffraction. At LANSCE, as described below, *polychromatic* pulsed neutrons are available. Since the time-of-flight of the neutrons determines the neutron wavelength, much smaller apertures or beam windows are sufficient.

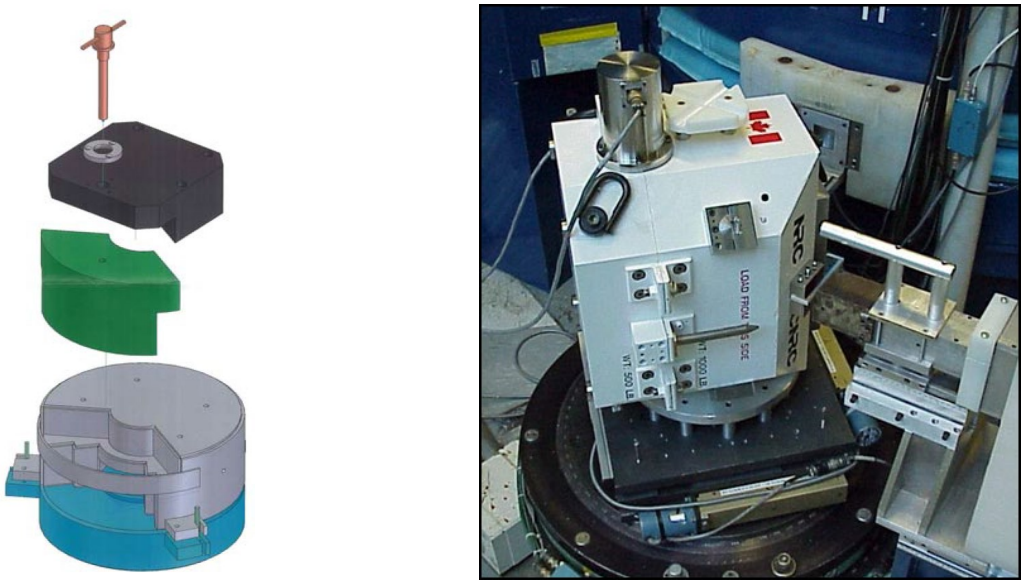

(a) (b)

Figure 2: (a) Schematic diagram of the castle used for the characterization of irradiated Al-U-7Mo (from [38]). The green volume is an 80° aperture that can be opened to allow diffracted neutrons of constant wavelength but different diffraction angles to reach the detector. (b) Photograph of the shielding apparatus used to characterize spent Al-U_3Si fuels by neutron powder diffraction at the Chalk River reactor (courtesy R. Rogge, Chalk River).

2.2 Neutron Resonance Absorption Spectroscopy

Neutron resonance absorption [41,42] allows to measure the isotope assay non-destructively and averaged over the sample volume illuminated by the neutron beam. It basically consists of a detector viewing a moderated pulsed source with the examined sample in-between, typically close to the source. This technique has been applied to spent nuclear fuel a few times as described below and was extensively reviewed and assessed for this application by Chichester & Sterbentz [43-45]. The technique was evaluated to characterize debris of melted fuel from the Fukushima accident [46,47] and the sensitivity can be improved by adding gamma detectors around the sample to detect the prompt gamma emission as a function of neutron energy (measured by time of flight) and emitted gamma energy [48].

The first report of the application of neutron resonance absorption spectroscopy is by Priesmeyer & Harz from 1975 [49,50]. Utilizing a fast chopper time-of-flight setup (maximum rotor speed: 12,000 rpm, minimum neutron pulse width 0.64 μs, flightpath length 42.93 m, eleven ^{6}Li glass scintillator detectors [51]) at the Geesthacht FRG-1 reactor, several samples with different enrichment and burnup were characterized for densities of ^{235}U, ^{238}U, ^{239}Pu, ^{131}Xe, ^{152}Sm, and ^{133}Cs. Samples were fuel platelets enriched to 45%, 55%, and 70% irradiated at Geesthacht, a sample from the research reactor in Petten, Netherlands, with a burnup resulting in 23% of ^{235}U remaining, as well as low enriched UO_2 fuel from a fuel rod and unirradiated UO_2 powder. Samples were placed in a cask with 17.5 cm lead shielding to all sides [51], allowing for sample in and out of beam measurements to determine the transmission, see Figure 3. The neutron energy range up to 200 eV was identified to be sufficient for resonance analysis. Radioactivities of about 600 Curie are reported for samples handled in this cask [51].

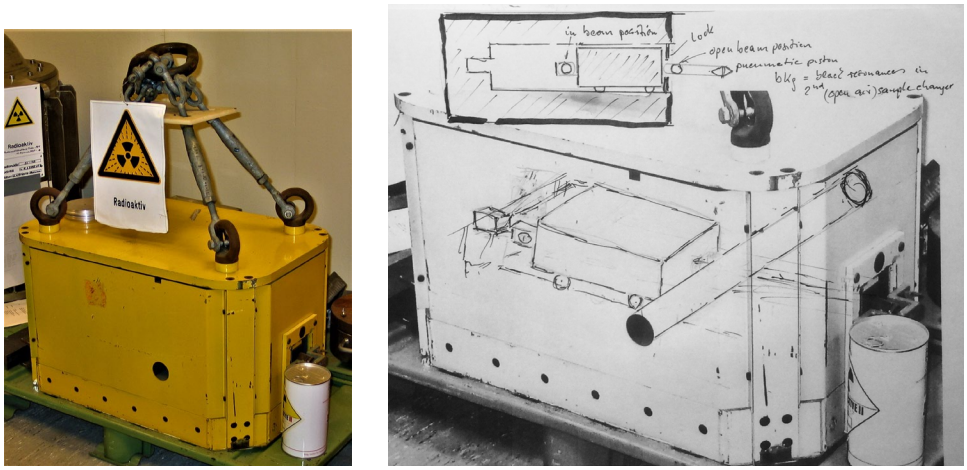

Figure 3: (a) Photograph of the handling cask used by Priesmeyer and Harz to characterize spent nuclear fuel by neutron absorption resonance spectroscopy in the early 1970s. (b) Sketch of the mechanism to allow for motion of the sample in and out of the beam within the cask (both pictures courtesy of Hans-Georg Priesmeyer, Geesthacht).

Using an electron linac producing 270 ns long pulses at 360 Hz hitting a tungsten target with polyethylene moderator, Bowman, Behrens and others characterized fresh and spent nuclear fuel at the National Bureau of Standards (now NIST) using neutron resonance absorption spectroscopy with a 22.21 m long flightpath [52,53]. The spent nuclear fuel samples were 2.5 cm long, 1.0 cm diameter cylinders cut from center and end of a fuel rod burned to ~25,000 MWd/ton in a commercial power reactor. Using the neutron energy range up to 40 eV, several uranium and plutonium isotopes were identified as well as ^{131}Xe, ^{133}Cs, ^{241}Am, ^{243}Am, ^{152}Sm, ^{145}Nd, and ^{99}Tc. A similar measurement for a fresh fuel allowed to compare the neutron results with the results of a destructive analysis and found agreements within error bars of both methods. The results allowed for instance to estimate that the neutron flux received by the sample from the end position of the fuel road was ~53% relative to that of the center position.

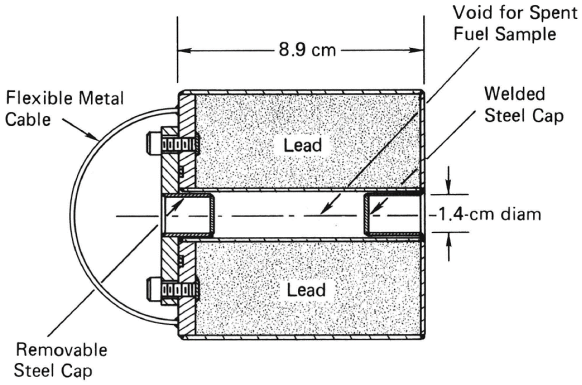

Figure 4: Shielding container used by Behrens et al. for the measurement of the isotopic assay in a 2.5 cm long, 1.0 cm diameter spent fuel sample (from [52]).

More recently, neutron absorption resonance spectroscopy was studied as a potential method to characterize the debris from melted debris after the Fukushima accident [46,47], but no actual characterizations could be found at the time of the writing of this report.

2.3 Neutron Radiography

While neutron diffraction or neutron absorption resonance spectroscopy on spent or irradiated nuclear fuel were only reported for the few cases described above, neutron radiography is somewhat more often applied to spent or irradiated fuel. The ability of neutrons to penetrate uranium, especially if depleted or low enriched, while at the same time being sensitive to hydrogen allows one to characterize several important aspects in fuel and cladding behavior during irradiation. The hydrogen sensitivity in particular allows one to understand cladding corrosion and accumulation of hydrides as important limiting factors for the achievable burnup. Some of the cases reported in the literature are described below. A common theme of the setups described here is the construction from two components: A transport cask which is placed on top of an "imaging block" with the fuel lowered below the transport cask into the imaging block to be exposed to the neutron beam with neutron radiographs recorded using the indirect dysprosium film exposure, more recently replaced with dysprosium doped image plates which can be scanned directly [54].

Neutron radiography is one of several PIE techniques utilized at PSI in Villigen, Switzerland [55]. A design to characterize 700 mm long, 10.8 mm diameter fuel rods was described by Groeschel et al. [56]. The strong gamma radiation from the highly radioactive samples required the use of dysprosium foils, significantly more sensitive to neutrons than gammas, to be used instead of more conventional detector for neutron radiography such as scintillator screens (since any X-ray sensitive converter medium would saturate by the radiation emitted from the sample even before neutrons arrive). The dysprosium foils activate with a long enough half-life that allows to expose them to X-ray sensitive film to transfer the neutron radiographs. The neutron radiography setup at the NEUTRA instrument at the spallation source SINQ (operated in constant-wave mode rather than as a pulsed neutron source, i.e. similar to a reactor) provided a L/D ratio of 350 with a beam flux of about 5×10^6 n/s/cm^2/mA [56]. An iron block with a vertical hole was added to improve the shielding at the NEUTRA beamline with the setup for characterization of irradiated materials dubbed NEURAP (for "Neutron Radiography of activated probes"). The fuel element, enclosed in a gas-tight Al capsule and transported in a transfer container, was installed into the hole. Motion control of a mounting head attached to the capsule allowed to lower the fuel rods into the neutron beam area and rotate in arbitrary positions for inspection of various angles. The radiography allowed to estimate enrichment based on the different attenuation of thermal neutrons by ^{235}U and ^{238}U. The same setup was also used to characterize spent SINQ spallation target rods where higher attenuation in the center of the target rods was found, which was explained by increased concentration of mercury due to differences in the proton beam profile hitting the target rods [24, 57].

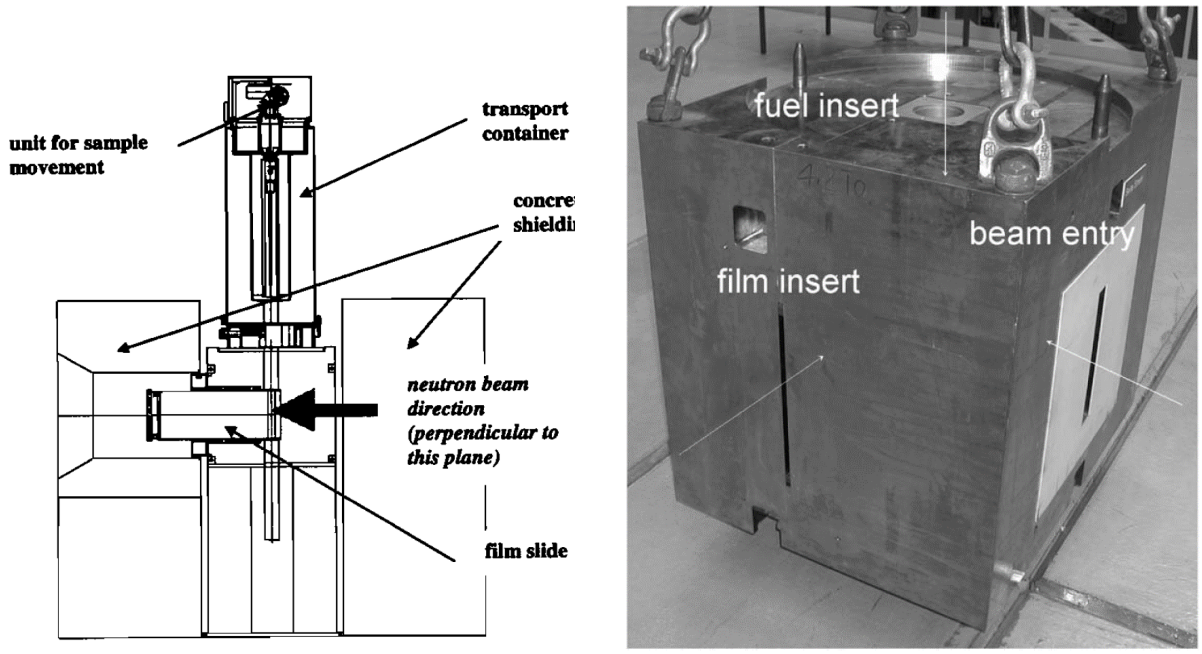

(a) (b)

Figure 5: (a) The NEURAP setup at PSI consisting of a steel shielding block with a hole to accommodate a 700 mm long, 10.8 mm diameter fuel rod docked on the upper part with a transportation cask (from [58]). (b) The shielding block with the center hole for the fuel pin, beam window and insert for a cassette with dysprosium film (from [24]).

Neutron radiography at the Institute for Energy Technology in Norway was performed extensively for fuel rods irradiated at the Halden reactor (HBWR) [23]. In a recent report, Jenssen et al. describe application of neutron radiography and tomography to characterize fuel response to ramp test and loss-of-coolant accident scenarios [23]. The sensitivity of neutrons to hydrogen was utilized to identify regions of hydrogen blistering among other characterizations (Figure 6). Dysprosium activation transferred to X-ray sensitive film was used to detect neutrons, same as for the PSI setup. No details on handling of the radioactive material were provided.

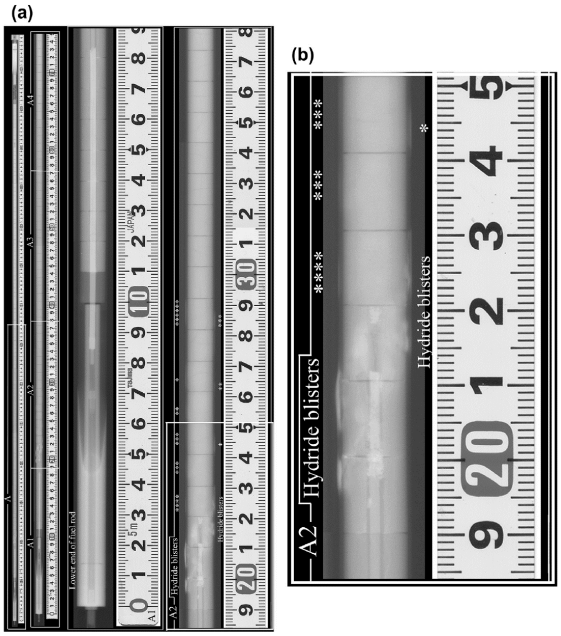

Figure 6: Neutron radiographs of fuel rods irradiated in a fuel degradation experiment at the Halden test reactor (a) with a magnified view showing hydrogen blistering (b) (from [23].

A setup similar to the PSI NEURAP installation is described by Singh et al. for evaluation of failed fuel rods at the neutron radiography station of the CIRUS reactor at the Bhabha Atomic Research Center (BARC) in Mumbai, India. As seen in Figure 7, three shielding casks with aligned center cavities are stacked vertically, allowing to illuminate different segments of a fuel rod with the dysprosium transfer technique used as an imaging modality in the center cask. Borated wax and lead bricks are used for shielding. The neutron beam tunnel cask and the middle shielding cask are made of a Pb-10wt%Cd alloy, shielding both gammas and neutrons. The beam tunnel cask is embedded in 350 mm thick borated wax as additional neutron shielding. Characterizations of experimental fuel rod designs as well as failed fuel rods are reported [30].

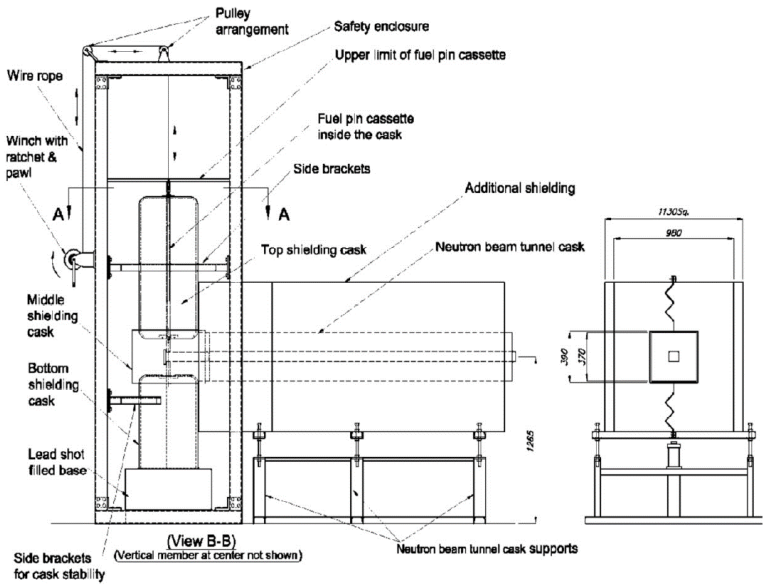

Figure 7: Schematic of the neutron radiography setup to characterize spent nuclear fuel rods by neutron radiography at the CIRUS reactor (from [30]).

Wei et al. describe in some detail a transfer cask enabling neutron radiography of irradiated nuclear fuel rods at the China Advanced Research Reactor (CARR) at the China Institute of Atomic Energy (CIAE) in China [25]. The radiography beamline offers up to 1×10^9 n/s/cm^2 with L/D ratios between 300 and 1200. Based also on the indirect imaging using dysprosium film, a setup including a transport container is described. Based on MCNP calculations for typical irradiated PWR fuel rod (15cm long, 33GWd/tU, ^{235}U enrichment 3.5%, decay time 1 year), a lead thickness of 13 cm was chosen to ensure a dose rate of 3 µSv/h (0.3 mRem/h). A mechanical gripper holds the fuel rod (Figure 8 (a)). To collect neutron radiography data, the container is positioned above the neutron beam on top of an "imaging block" and the fuel rod is lowered below the cask into the imaging block, exposing it to the neutron beam (Figure 11 (b)). The imaging block is a 90 cm cube of 2cm wall thickness steel filled with heavy concrete (4.6 g/cm^3) with appropriate cavities for the incident neutron beam and a slot perpendicular to the beam to insert cassettes with dysprosium film. The setup is similar to the NEURAP setup described above. Although the cited paper was published in 2013, according to Google Scholar at the time of the writing of this report, no citations indicating actual application to characterize a nuclear fuel exist.

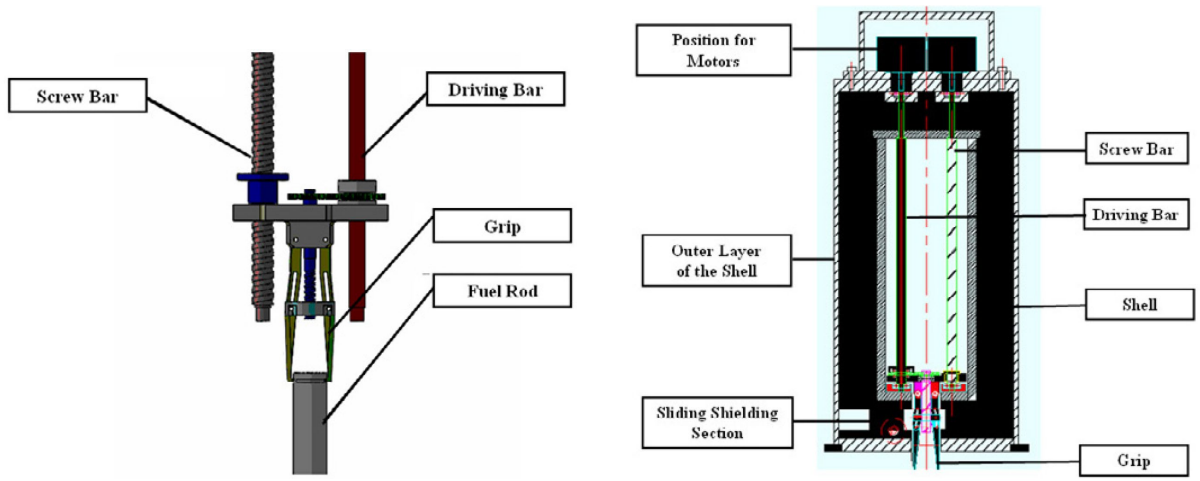

(a) (b)

Figure 8: (a) Mechanical gripper using claws to hold a fuel rod and screw bars to move the gripper for the transport container for irradiated fuel rods designed at CARR. (b) Schematic of the transport container. The fuel rod is lowered to below the cask into the neutron beam through a hole in the bottom of the container (from Wei et al. [25]).

The PIE and neutron radiography capabilities at INL are described in more detail below.

3. Experimental Methods

This section provides brief descriptions of the capabilities involved and the instruments utilized. A description of the prototype design of a cask allowing to handle and characterize irradiated nuclear fuels at LANL in the future was reported in a second report for FY20.

3.1 Facilities at Idaho National Laboratory (INL)

Facilities located at INL include fuel fabrication, pre-irradiation characterization, irradiation at the Advanced Test Reactor (ATR) or Transient Reactor Test (TREAT), and post-irradiation examination at various facilities located at INL's Materials & Fuels Complex (MFC) [59]. Fuels and other nuclear materials fabricated at the Materials & Fuels Complex or elsewhere are sent to the Advanced Test Reactor where they are irradiated under steady state, representative or prototypic conditions. Fresh or irradiated fuel can also be irradiated under transient or low power steady state conditions at the TREAT reactor. The irradiated fuels are then returned to the Hot Fuels Examination Facility (HFEF, Figure 9) at the Materials & Fuels Complex (MFC) where they undergo a variety of nondestructive examinations prior to destructive examinations. Irradiated fuels studied at INL are often fabricated, irradiated, and examined on site. In addition, INL is also able to receive nuclear fuels irradiated at other reactors for examination [60-62]. Once the irradiated fuels arrive at the Hot Fuels Examination Facility, non-destructive examinations that may be performed include visual examination, neutron radiography and tomography, dimensional inspection and profilometry, precision gamma scanning (PGS), and eddy-current examination [63].

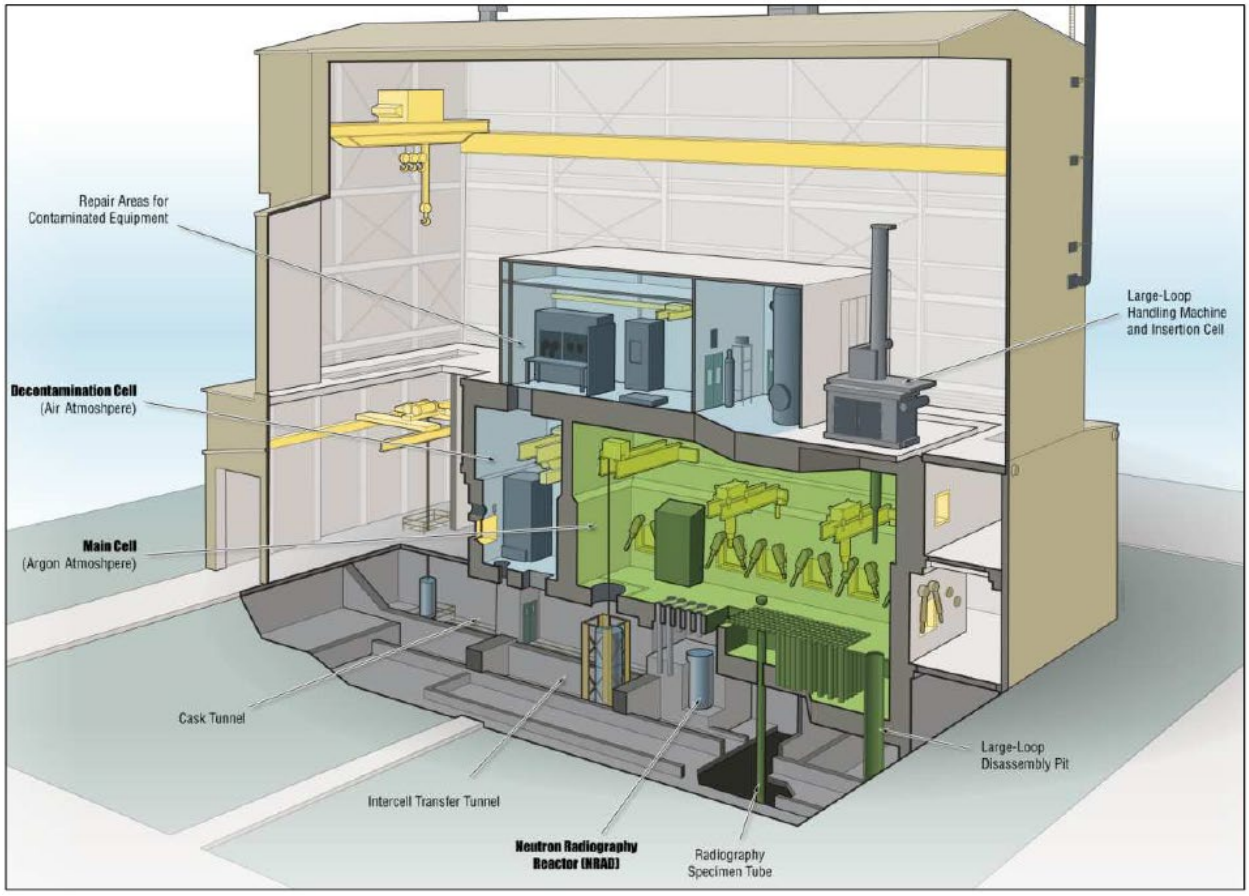

Figure 9: Cut-away view of the Hot Fuels Examination Facility (HFEF) showing the layout of the hot cells and the NRAD facility below (from Craft et al. [64]).

The Neutron Radiography Reactor (NRAD) is a 250 kW_{th} research reactor located beneath the HFEF main cell that has two neutron beamlines specifically designed for neutron radiography and tomography of irradiated nuclear fuels [64]. Figure 10 shows the layout of the two neutron radiography beamlines at NRAD, one routing to the East Radiography Station beneath the hot cell and the other routing north to the North Radiography Station. An elevator between the HFEF main cell and the East Radiography Station allows samples in the main cell to be remotely lowered into the neutron beam for neutron radiography and tomography. The North Radiography Station is not beneath the main cell but is equipped with an elevator and a cask mounting system such that samples brought to NRAD with a cask can be remotely lowered into the neutron beam for neutron radiography and tomography. Both the East and North Radiography Stations are equipped to perform transfer method neutron radiography using activation foils (dysprosium for thermal neutrons and cadmium-filtered indium for epithermal neutrons) with both film and X-ray photostimulable phosphor image plates [65]. Additionally, the North Radiography Station is equipped with a digital camera-based neutron imaging system that is able to perform digital neutron CT of lightly irradiated specimens. Recent experiments performed neutron CT on an ATF rodlet after it underwent transient testing at TREAT, producing 1081 neutron radiographs of the specimen in 18 hours. This sample emitted only 150 mR/h on contact, which was low enough to allow for direct digital neutron tomography.

It is pertinent to mention that the neutron radiography and CT capabilities currently available at Hot Fuels Examination Facility [66] do not assess isotope distributions or microstructural features such as crystallographic phases, texture or strain, which might be accessible using pulsed neutron characterization.

These non-destructive examinations inform researchers about locations suitable for subsequent detailed destructive examinations. Samples may be prepared for metallography/ceramography, physical properties testing (e.g. thermal properties, density), chemical analysis, isotopic analysis, alpha/beta/gamma spectrometry, mass spectrometry techniques, mechanical property testing, and other analyses. These examination capabilities are available at other facilities co-located at the Materials & Fuels Complex.

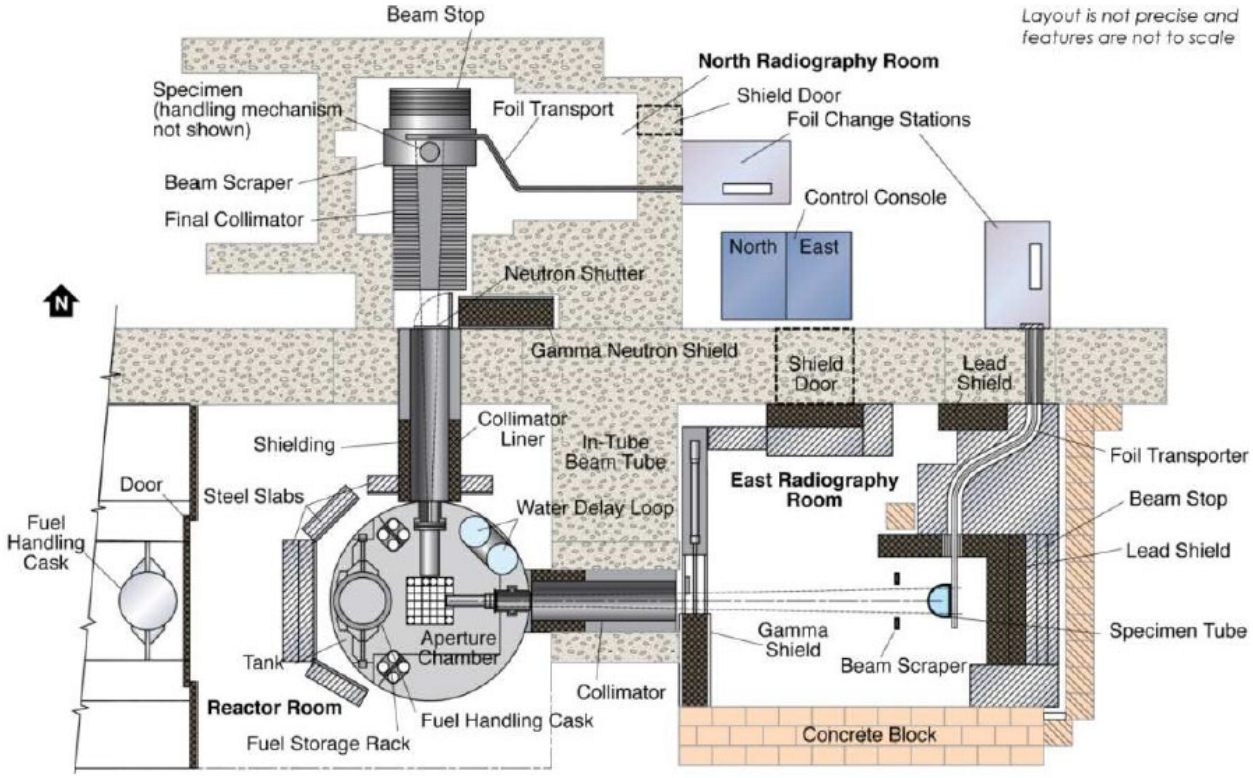

Figure 10: Floor plan layout of the neutron radiography facility NRAD with the two neutron beam lines (from Craft et al. [64]).

3.2 Facilities at Los Alamos National Laboratory (LANL)

At present, the neutron methods described here require large scale user facilities such as LANSCE. Besides providing the required neutron instruments, these facilities also have to have the authorization basis, infrastructure and experience to handle such materials. While international shipment of such materials is not impossible, for example the spallation neutron source at J-PARC, Tokai, Japan, is not authorized to handle even depleted uranium. Handling of these materials in the U.S. is regulated by a materials at risk (MAR) assessment of the samples [67,68]. This assessment takes into consideration several hazard management aspects of the materials, including radioactivity, and results in a MAR expressed in "plutonium equivalent grams" (PEG). Facilities have designated MAR limits for their total inventory. At LANSCE, the Manual Lujan Scattering Center, where HIPPO and FP5/ERNI described below are located, has a MAR limit of 380 PEG, while the Weapons Neutron Research (WNR, unmoderated spallation neutrons) and proton radiography (pRAD) facilities at LANSCE have limits of 40 and 12 PEG, respectively. For comparison, the SNS requires a case-by-case approval by the Department of Energy for experiments involving MAR samples. In this combination of pulsed neutron characterization capabilities with an authorization basis that allows handling of all fuel forms, LANSCE at LANL is unique world-wide as e.g. documented by the characterization of the U-20Pu-10Zr-3Am-2Np sample [13].

3.2.1 Neutron Diffraction

For time-of-flight neutron diffraction characterization of nuclear fuels the HIPPO (High Pressure/Preferred Orientation) beamline at LANSCE is utilized [69,70]. Figure 11(a) provides a schematic of the instrument. The comparably short distance of 8.83 m between moderator and sample combined with the comparably large detector coverage of 22.4% of the sphere around the sample [71] provides for efficient neutron diffraction characterization. A robotic sample changer [72] is used to handle samples inside the instrument (Figure 11 (b)). In combination with a 2 mm Cd slit to define a slice of the sample, the robotic arm allows to scan rodlets with several pellets in 2 mm slices, thus providing limited spatial resolution for the diffraction. Data analysis is conducted with the Rietveld method, fitting every experimental data point to a complex (several tens of parameters) model taking into account instrument parameters (e.g. time-of-flight to d-spacing conversion, background, instrument peak broadening), crystallographic parameters (e.g. lattice parameters, atomic positions, atomic displacement parameters), and microstructural parameters (texture/preferred orientation, phase fractions, defect concentrations). Figure 12(a) shows an example of a Rietveld analysis of a 2 mm slice of a UN/U_3Si_5 sample inside a stainless steel rodlet. Figure 12(b) shows the refined unit cell volume (many other refined parameters are omitted here) of the hexagonal crystal structure of U_3Si_5 as a function of sample position along the rodlet. The data points corresponding to the lowest pellet are significantly below those of the other pellets, indicating an anomaly for this particular pellet. Measurement of the crystal orientation distribution (texture, preferred orientation) shows that while the UN crystals show the expected random orientation distribution (absence of preferred orientation), the U_3Si_5 shows a very strong texture consistent with essentially two single crystals within the probed volume, Figure 12(c). This can be explained that this particular pellet was unintentionally exposed to a slightly higher temperature during the sintering than the melting point of the U_3Si_5. Upon cooling, the U_3Si_5 solidified in an interconnected network surrounding the UN grains, but forming the two single crystals seen now. It is worth pointing out that this pellet, fabricated during the development of synthesis routes for this particular fuel form, passed visual inspection and did not show any differences in density prior to insertion into the capsule. Anisotropic thermal expansion along the crystallographic a- and c-axes of the hexagonal crystal lattice may lead to thermal stresses that could cause cracking of this pellet during heating, significantly changing the behavior during irradiation. This example underlines the value that bulk neutron characterization can provide for pre-irradiation characterization, but also for the development of fabrication routes. Besides pre- and post-irradiation characterization, neutron diffraction also has significant advantages to characterize crystal and microstructure evolution of nuclear fuels at temperature, atmosphere, processing route etc., e.g. for separate effect testing.

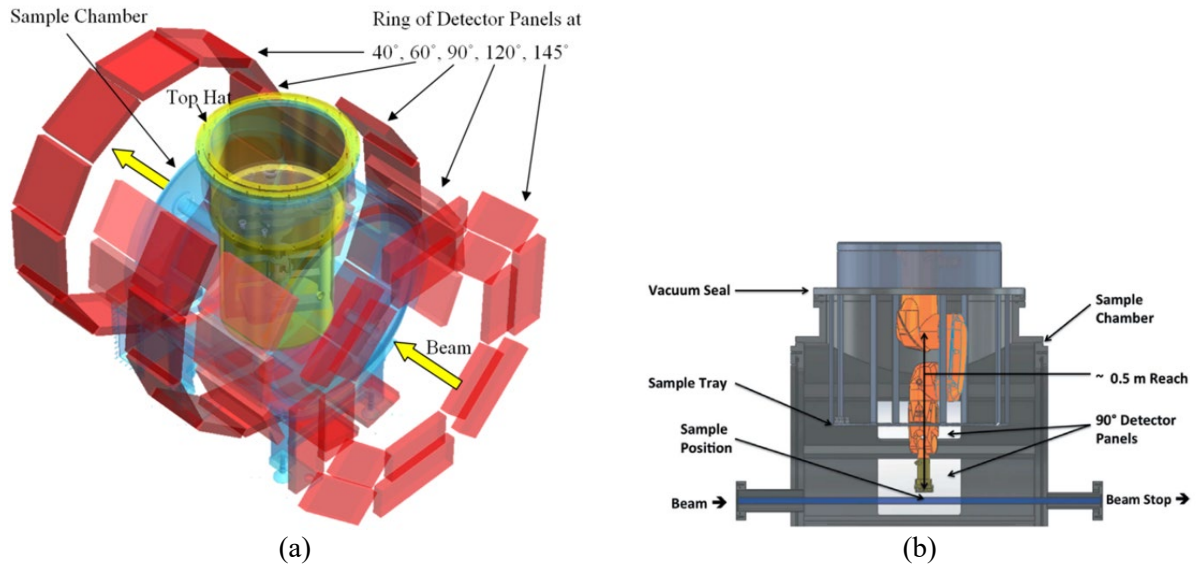

Figure 11: Schematics of the HIPPO instrument (a) and the robotic sample changer (b).

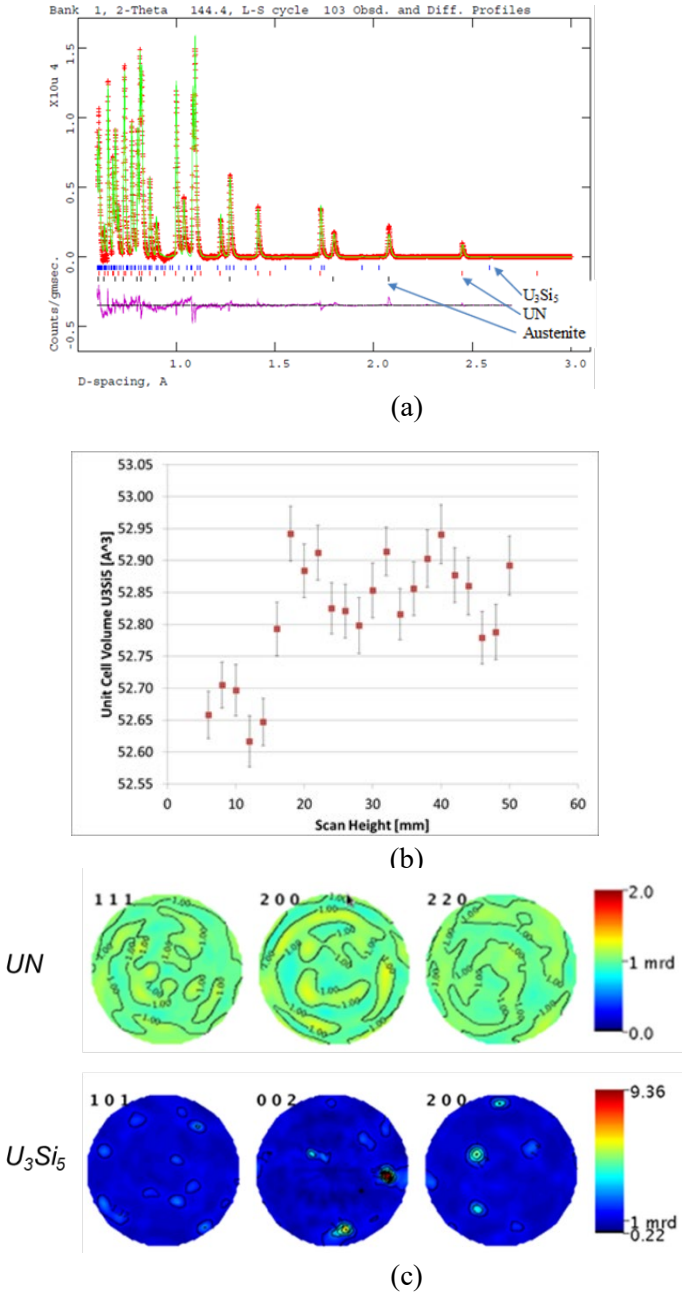

Figure 12: (a) Example of a Rietveld full pattern diffraction data analysis of HIPPO data on an UN/U_3Si_5 composite fuel inside stainless steel cladding. The red crosses are measured intensities, the green line is the Rietveld fit, the tick marks below the pattern label calculated peak positions for the phases indicated. The difference curve for the data shown as intensity vs. d-spacing is shown below. (b) Unit cell volume of the hexagonal U_3Si_5 phase resulting from lattice parameter refinements as a function of scan height, indicating that the data points corresponding to the first of the three pellets scanned are significantly lower than the average. (c) Pole figures of a texture analysis measuring the grain orientation in the probed volume. While the UN grains show a random grain orientation (absence of preferred orientation), this data indicates that the U_3Si_5 phase has a microstructure similar to a single crystal with essentially two main orientations for crystallographic c-axes (002 pole figure) and two sets of maxima each of the three a-axes visible for each orientation.

3.2.2 Energy-resolved Neutron Imaging and Computed Tomography

Located next to the HIPPO beamline is the energy-resolved neutron imaging (ERNI) beamline on flight path 5 [73] at the Lujan Center. Similar to HIPPO, the ERNI beamline takes advantage of the same pulsed neutrons coming from the high intensity moderator on the 1L target [74]. For a schematic layout of the ERNI beamline on flight path 5, see Figure 13(a). Using this pulsed neutron source, along with a pixilated neutron time-of-flight detector, neutron radiographs can be further separated out based on the time-of-arrival, or energy, of each incoming neutron (Figure 13(b)). The detector used for ERNI measurements consist of neutron-sensitive microchannel plates (MCPs) coupled to four Timepix readout chips (see schematic Figure 13(c)), combining to a total active area of 28mm x 28mm [75,76]. This type of detector setup is capable of producing highly pixelated (512x512 at 55um pitch) neutron radiographs with time resolution as high as ~20 ns with some limitations on part of spectrum which can be covered in one measurement. Roughly 3K frames per neutron pulse can be acquired at the Lujan Center. The ongoing development of the next generation detector at UC Berkeley should substantially improve its capabilities, specifically for energy-resolved neutron imaging. Combining this type of detector to the pulsed neutron source at the Lujan Center opens up avenues for several novel applications for material characterizations, ranging from specific isotope mapping [16], including fission gases [17] to bulk temperature mapping [77].

(a)

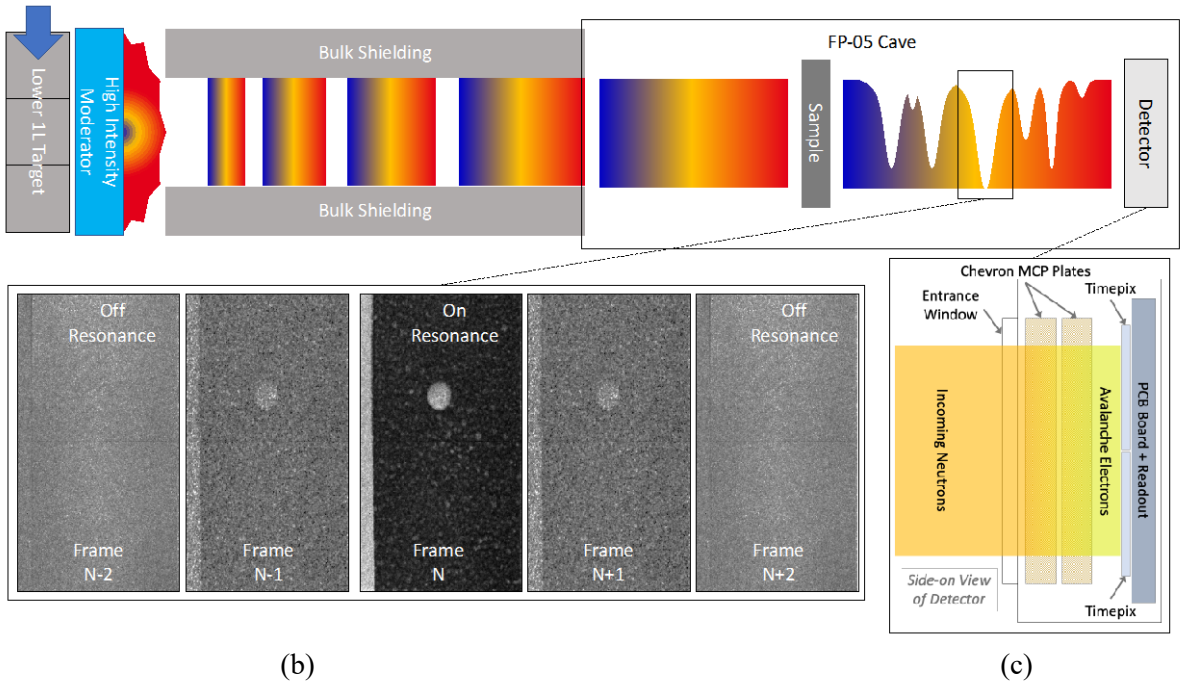

(b) (c)

Figure 13: (a) Schematic of flight path 5. (b) Examples of radiographs collected at energies around a neutron absorption resonance. (c) Schematic of the pixilated time-of-flight imaging detector.

A typical energy-resolved neutron imaging experiment involves transmission measurements, where neutrons passing through a given sample interact with the material based on neutron cross-sections of the isotopic constituents within the material. These interactions absorb a certain number of neutrons at specific energies, so called neutron absorption resonances, as they pass through the sample, thus resulting in observable dips in the transmission spectrum recorded by a TOF detector at these energies. The depth and position of these transmission dips act as a finger print for the isotopic composition of the sample. Using modern reaction-theory codes, such as SAMMY [78,79] or REFIT [80], transmission spectra can be fit as a function of energy to extract quantities like isotopic areal densities. This transmission fitting procedure can be done on a pixel-by-pixel basis, thus producing a 2D map of specific isotopic density distributions

for each isotope within the sample. Furthermore, by recording and extracting 2D isotopic densities over a range of sample rotations, a 3D isotopic distribution map can be obtained through computed-tomography techniques. An example of this is shown in Figure 14, where UN/U-Si composite fuels were imaged using ERNI techniques over ~60 sample rotations. Transmission spectra with absorption resonances from ^{235}U and ^{238}U within the transmission spectra were fitted using SAMMY to extract areal densities of ^{235}U and ^{238}U for each pixel in each sample rotation image. These isotopic density maps of ^{235}U and ^{238}U are processed by a CT-reconstruction software [81] to ultimately create 3D density maps of ^{235}U and ^{238}U within the probed pellets. It has been demonstrated that this technique can not only be qualitative, but also a quantitative probe in actually measuring isotopic contents in atomic percent levels [13].

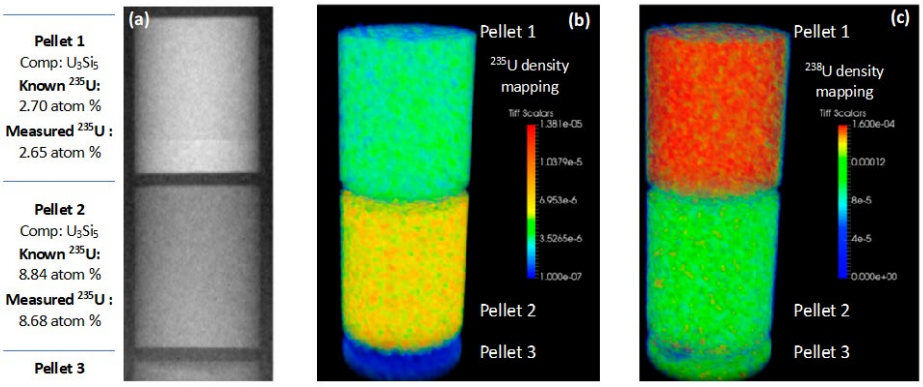

Figure 14: Thermal neutron radiography (a) and reconstruction of ^{235}U (b) and ^{238}U (c) isotope densities in uranium silicide fuel pellets with different enrichment levels.

Recently, it was demonstrated that neutron radiography of irradiated fuels assemblies can be performed with an equivalent detector system despite the very intense radiation fields produced by the fuel that make their post irradiation examination very difficult [82,83]. The neutron imaging detector, equivalent to the one used at the FP5 beamline, comprised of microchannel plates (MCPs) and a Timepix readout, was tested in intense gamma and neutron radiation environments on a beam line at the Neutron Radiography Reactor (NRAD) at Idaho National Laboratory [82]. Initially, neutron radiography experiments of non-irradiated materials were performed with the detector installed 17.5 m from the reactor core in a line of sight view to the core of the reactor. Therefore, the detector was exposed to a fast and epithermal neutron spectrum as well as high intensity gamma radiation. The gamma-ray dose rate in the beam line was 812 mSv/hr. Complementary measurements were made using ^{137}Cs and ^{60}Co isotopic sources at gamma dose rates in excess of 6 Sv/hr. The detector functioned normally over several hours in this environment. These measurements were followed by the imaging of an irradiated fuel assembly with the detector installed at 4.8 m from the reactor core, again with direct view onto the reactor core [83]. A 75-cm long fuel assembly was positioned ~4 cm from the detector during neutron radiography. The radiation generated by the fuel assembly at the detector position was 5.48 Sv/h. A set of neutron transmission images was acquired by the detector, which could operate in these high radiation environments despite several recoverable single event upsets observed in the FPGA processing electronics.

These experiments demonstrated that high resolution imaging of irradiated fuel assemblies is possible with digital detectors, which can extend the capabilities of non-destructive studies to many advanced imaging techniques such as tomography, resonance absorption and Bragg edge imaging dark field imaging and others. These conditions are comparable to planned radiography of irradiated nuclear fuel assemblies reported here, however, with a pulsed source the time during which the detector is active can be reduced to the neutron time-of-flight of interest, thus greatly improving the signal to noise ratio.

3.2.3 Neutron Absorption Resonance Spectroscopy

The recently installed high rate ^{10}B liquid scintillator detector [84], located in the 60 m station of FP5, is in the process to become fully operational. Dedicated data acquisition electronics for all 55 channels were purchased in FY19 and were installed during the LANSCE down time in the summer 2020, after the measurements described below, which were conducted with borrowed data acquisition equipment. This detector will improve the efficiency at higher neutron energies compared to the imaging detector as well as improve the energy resolution due to the longer flightpath length. With a smaller collimation (mm sized instead of cm sized) this will allow interrogation of regions of interest identified with the imaging setup and aligned in the beam with the motion control equipment of the imaging beam line, providing a unique advantage of a combined material science/radiography and nuclear physics setup for enhanced material characterization. Either collimation or sample should ideally be movable to allow aligning a sample region of interest after a bulk CT for detailed characterization with resonance spectroscopy.

4. Sample AFC-3A-R5A

The material available at LANSCE for characterization was cut as a ~6mm diameter, 1.5 mm thick disk-shaped sample from the AFC-3A-R5A fuel slug. The ICP-MS chemistry and isotopics of this sample prior to irradiation, i.e. the fresh fuel, are listed in Table 1.

Isotope/Element	Weight %.
U-total	90.97
U-233	0.00
U-234	0.51
U-235	51.41
U-236	0.30
U-238	38.76
Pd	1.4
Mo	0.00
Zr	7.63
C	0.00

Table 1: Pre-irradiation Isotopic and elemental composition of the sample cut from the AFC-3A-R5A fuel slug, with a nominal composition of U-10Zr-1Pd. The enrichment level with U-235 was 56.51%.

The fuel was irradiated as part of the Nuclear Technology Research and Development (NTRD) Advanced Fuel Campaign (AFC) program at ATR to a burnup of 2.5 %FIMA and is provided to the team for the duration of the NSUF funded experiment. The sample is a ~1.5 mm thick slice cut from an irradiated U-10Zr-1Pd fuel slug with ~6mm diameter. The sample is held in an aluminum holder specifically designed for this sample by INL and LANL and built at INL. The aluminum holder is attached to a flange that can be inserted into a 9mm vanadium can that provides secondary containment to prevent contamination, sample orientation, and the ability to attach the sample to the standard sample changer used at LANSCE (see Figure 15). The sample setup has been conducted in hot cells at INL with the outer vanadium can decontaminated for handling. The sample arrived at LANSCE November 22, 2019, allowing for testing of the developed procedures and some initial characterization before the LANSCE beam cycle ended in December 2019. More detailed characterizations are planned in the 2020 run cycle.

Figure 15: Opened aluminum sample holder with the cavity for the disk of irradiated U-10Zr-1Pd in the thinned section (a) .Sample holder closed and attached to the lid of a vanadium can that provides secondary containment of the sample.

Isotope	*Mass(g)*	*Mass %*
U234	0.00193389	0.44%
U237	1.2911E-13	
Np238	1.9108E-17	
Np239	1.9051E-15	
Am241	2.2882E-07	
Cm242	1.4074E-10	
Sr89	5.7401E-07	
Sr90	0.00021246	0.05%
Y90	5.3114E-08	
Y91	1.5711E-06	
Zr95	2.7144E-06	
Nb95	3.2239E-06	
Nb95m	1.1355E-09	
Ru103	8.7689E-08	
Rh103m	7.869E-11	
Ru106	1.8644E-06	
Te129	4.7829E-13	
I131	2.8489E-19	
Cs137	6.4635E-05	0.01%
Ba140	9.7655E-14	
La140	1.4797E-14	
Ce141	2.0805E-08	
Pr143	3.3607E-13	
Ce144	2.4002E-05	0.01%
Pr144	1.0128E-09	
Nd147	1.5325E-15	
Pm147	1.9138E-05	
Zr	0.04502262	10.16%
Pd	0.0114067	2.57%
U235	0.20596968	46.49%

U238	0.17675198	39.90%
Pu238	2.1054E-05	
Pu239	0.00147193	0.33%
Pu240	8.188E-05	0.02%
Pu241	9.6889E-06	

Table 2: Complete list of isotopes predicted after irradiation for a decay date of 4/21/2013, i.e. several years prior to the characterizations described below. Mass percent with less than 0.005% were removed for clarity.

5. Shipping to LANL and Handling at LANSCE

The sample was shipped in a Model 8500 shipping cask from INL to LANL. The main shielding component of this cask is depleted uranium. Figure 16 shows a drawing of the main components of the cask.

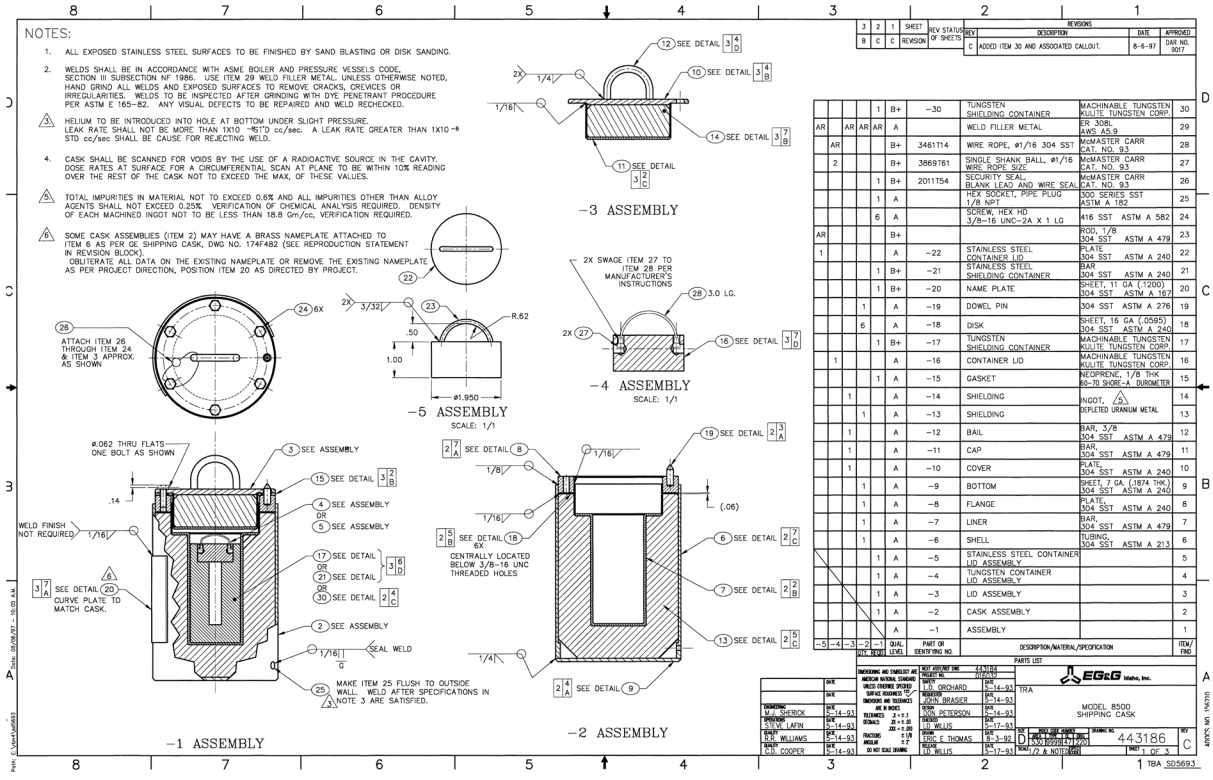

Figure 16: Drawings of the cask used to send the irradiated fuel sample to LANL.

At LANL, an integrated work document (IWD) was developed to handle the sample. After initial measurement of the dose rate it was concluded that the dose rate does not require working under a radiological work permit and that the IWD is sufficient. Two meter long remote handling tongs, Figure 17, were used to provide safe distance of the operator from the sample. At this distance, dose rates of 10 mrem/hr or less were observed, rendering this mode of operation acceptable.

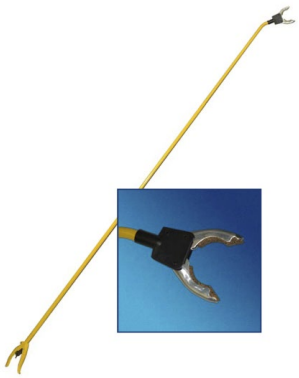

Figure 17: Remote handling tongs used to handle the sample at LANSCE. Tongs provided by QSA Global, Inc., Baton Rouge, LA. Total length is 2 meters.

6. Preliminary Results

After the sample arrived Friday 11/22/2019, towards the end of the 2019 LANSCE run cycle ending on 12/21/2019, some limited beamtime was spent on HIPPO and FP5 to exercise the developed handling procedures and collect some preliminary data on the U-10Zr-1Pd sample. These measurements were conducted in preparation of much longer, NSUF funded beam time planned in the 2020 LANSCE run cycle. These preliminary measurements are reported here, mostly to illustrate the type of information to be gained from these experiments. No scientific conclusions can be drawn from these early results at this point.

6.1 Neutron Diffraction

The sample was characterized in the HIPPO beamline as shown in Figure 11. The high enrichment level of the sample, 56 at% U-235 prior to irradiation, results in strong absorption of thermal neutrons, which makes diffraction difficult. Consequently, while the signal from the aluminum sample holder is fairly strong, the diffraction from the actual sample is comparably weak. Figure 18 shows data collected for 45 minutes with the 90° detectors. The signal is dominated by strong peaks from the aluminum sample holder, with some weak peaks not accounted for by the peak positions of the aluminum. Figure 19 shows the same data re-scaled to show these weak peaks more clearly.

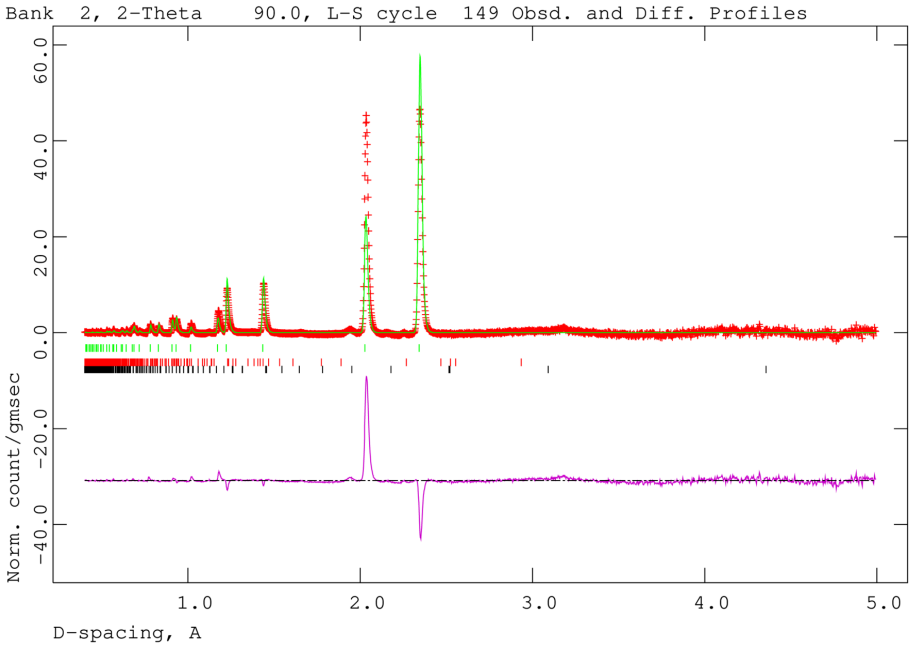

Figure 18: Diffraction signal of the 90° detector ring of the HIPPO diffractometer. The measured data is shown as red "+" symbols, the Rietveld fit is shown as a green line through the diffraction data and the difference curve is below. The tick marks indicate calculated diffraction peak positions for peaks of δ/ω-UZr_2 (lowest row, black), α-U (second row from bottom, red), and aluminum (top row, green).

Figure 20 shows typical dU-10Zr diffraction patterns obtained during cooling of a samples from the γ-phase region for comparison from a previous study on HIPPO [85]. This sample was made from depleted uranium and therefore did not suffer from the strong absorption of thermal neutrons used for diffraction experiments. In this work, ~81 wt% α-U and ~19 wt% δ/ω-UZr_2 were found by Rietveld analysis of the diffraction data, in agreement with the phase diagram. See references [86] and [87] for information on the relevant phase diagram and descriptions of the crystallographic phases. The data illustrates that signature peaks of α-U are the triplet of peaks occurring at ~2.5 Å (visible as two peaks with a shoulder towards low d-spacing on the left peak). The second phase present, the δ/ω-UZr_2, has typical peaks at ~1.9Å and another weak peak at ~3.1Å.

While a detailed Rietveld analysis of the data of the irradiated sample has not occurred yet, Figure 18 and Figure 19 show by comparison of the calculated peak positions for the δ/ω-UZr_2, (black tick marks, bottom row) and α-U phases (red tick marks, middle row) that peaks for α-U, which should be the dominant phase, appear to be absent, especially the strong signature peaks around 2.5Å in d-spacing. On the other hand, a comparably strong peak occurs at ~1.9Å and a weaker one at slightly less than 2.2Å, both peak position of δ/ω-UZr_2. More work to match the peak positions of these phases better is required. A much longer data acquistion time on HIPPO, providing much better statistics, will be conducted for the full measurement. However, the preliminary results seem to indicate that δ/ω-UZr_2 is present while α-U appears to be absent in the irradiated U-10Zr-1Pd sample. A sample of a non-irradiated U-10Zr-1Pd would be needed to verify whether the addition of ~1 wt% Pd changes the phase composition compared to binary U-10Zr without Pd.

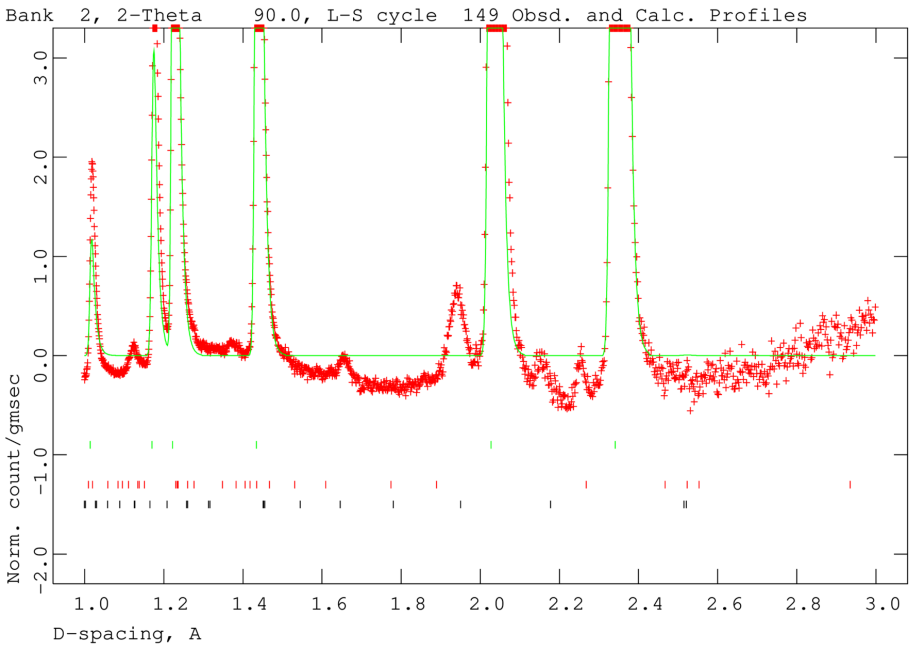

Figure 19: Diffraction signal of the 90° detector ring of the HIPPO diffractometer re-scaled to show the weaker diffraction signal from the sample. The measured data is shown as red „+" symbols, the Rietveld fit is shown as a green line through the diffraction data and the difference curve is below. The tick marks indicate calculated diffraction peak positions for peaks of δ/ω-UZr$_2$ (lowest row, black), α-U (second row from bottom, red), and aluminum (top row, green).

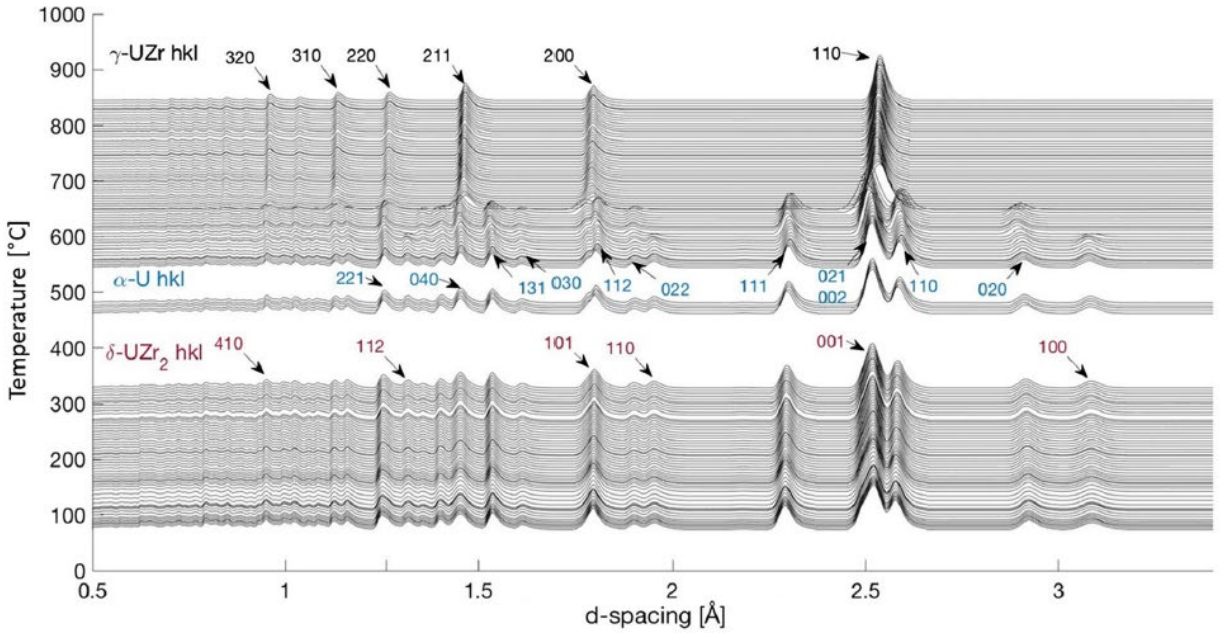

Figure 20: Diffraction patterns of a dU-10Zr sample during cooling from the γ-field, also collected on the HIPPO diffractometer for a different study for comparison (from [85]). Peak positions of several γ-U, α-U, and δ/ω-UZr2 are indicated. Note that the α-U phase occurs before (~650 °C) the δ/ω-UZr$_2$ phase (~600 °C) during cooling. Best indicators for presence of the δ/ω-UZr2 are the (110) and (100) peaks at ~1.9Å and ~3.1Å, respectively, while the peaks around 2.5Å are predominantly from α-U. The refined weight fraction for this sample at the lowest temperature for α-U and δ/ω-UZr$_2$ are ~81 wt% and 19 wt%, respectively.

6.2 Energy-resolved Neutron Imaging

The specific setup of the measurements for the U-10Zr-1Pd sample on FP5 utilized for these measurements is shown in Figure 21. Here, as the neutrons travel down the flight path from the high intensity moderator located at the 1L target, the beam is collimated down to ~2 cm using a set of collimators ("D-collimation" in Figure 21) located directly upstream of the entrance to the FP5 cave. Within the FP5 cave, neutrons are then transmitted through a removable tantalum plate to create opaque resonances to help with background characterization and energy calibration. After the collimation and the Ta calibration plate, the neutron beam goes through up to two additional sets of collimators. The first is a scraping collimation which meant to clean up any background within the neutron beam. The second set of collimation is a 25 cm long, 1mm opening brass collimator, which was used only for a sub-set of measurements on the U-10Zr-1Pd sample to probe only a much smaller volume of the sample. After going through these additional collimators, neutrons then impinge upon the U-10Zr-1Pd which is held in place using a 3-axis motion stage (rotation, horizontal, and vertical translation) for sample alignment. Directly downstream from the sample was the MCP-Timepix detector. For these measurements, electronic shutters were configured to cover 30 μs to ~650 μs neutron time of flight values, which cover epithermal energies. With a flight path length of ~ 9 meters, this time-of-flight range translates to an energy range of ~1 eV to ~500 eV. Even though the time-of-flight resolution is constant, the corresponding energy resolution degrades as neutron energy increases, thus the ability to resolve neutron absorption resonances at higher energies (> 100 eV) becomes difficult and a longer flight path length is needed. Moreover, quantification of resonances at energies above 100 eV at the present setup is difficult due to a large fraction of background signal arriving at the detector, which dominates the measured neutron flux at higher energies. The background in the 60m silo station is substantially lower due to the larger distance from the source.

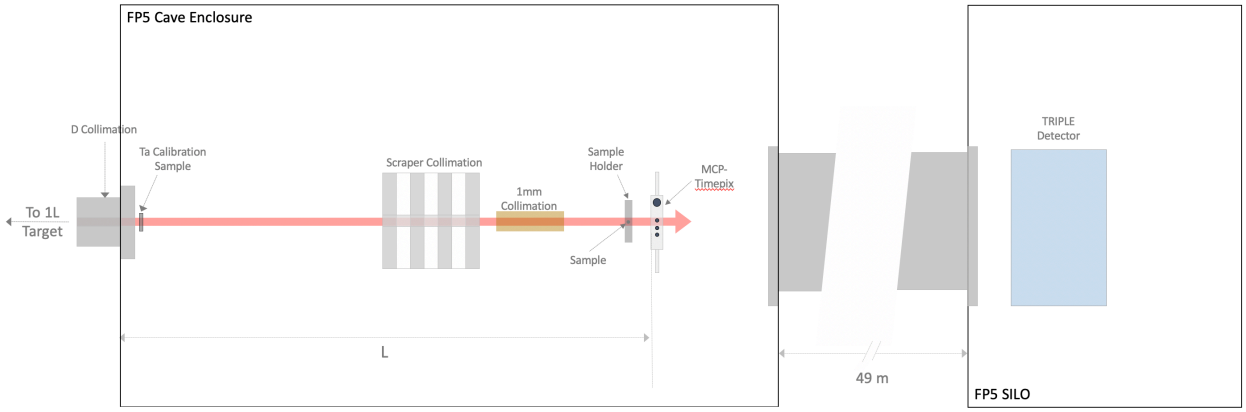

Figure 21. Setup of ERNI measurements on FP5 with the irradiated U-10Zr-1Pd sample during the 2019 LANSCE run cycle. On FP5 there were two stations performing measurements simultaneously. The main ERNI measurements were performed in the FP5 cave with the MCP-Timepix detector, while additional neutron resonance transmission analysis was performed in a parasitic mode with the TRIPLE detector at the FP5 silo station at a moderator to detector distance of ~60m.

In addition to the ERNI measurements within the FP5 cave enclosure, the TRIPLE collaboration detector was operated at the 60 meter so-called silo station during this time. The 60 meters distance from the 1L target allows for much better energy resolution while the 4cm layer of liquid scintillator provides a detector efficiency of still 71% at a neutron energy of 1 keV. This setup allowed neutron resonance transmission analysis (NRTA) measurements to be performed on the U-10Zr-1Pd sample in tandem with the ERNI measurements (the energy-dependent beam attenuation from the imaging detector in the cave is negligible once the data is normalized to the open beam). Although there is no spatial resolution besides selection of ~1mm^2 areas using the brass collimator, neutron energies up to 10 keV are accessible for NRTA with this detector. This allows for better identification of lighter isotopes with resonances in the ~100s of eV range,

like zirconium, as well as better characterization of resonances that are overlapping when measured at 9m etc.

In total there were four distinct setups where both the MCP-Timepix and TRIPLE detector were simultaneously used to record measurements. The first was without the use of the 1mm collimation setup, which yielded a beam spot of ~15 mm diameter on the MCP-Timepix detector that fully covered the sample. The final three used the 1×1 mm^2 collimation placed ~25 cm upstream of the sample. This collimation was specifically built for this experiment and due to the length of the 1×1 mm^2 slit (10 cm in order to provide sufficient attenuation of unwanted neutrons and gammas), alignment with the beam is key. The imaging detector can be used to verify the selected volume on the sample. With this 1mm collimation setup, the sample was moved vertically through the beam, with two images resulting in only half of the sample being illuminated with neutrons. Summed image stacks, equivalent to white beam exposure, from the MCP-Timepix detector for each of these three setups are shown in Figure 22. At this time it is somewhat unclear why the 1mm collimation resulted in a >6mm diameter beam spot. Potentially the distance between collimation and sample contributed. This will be explored further in the 2020 run cycle.

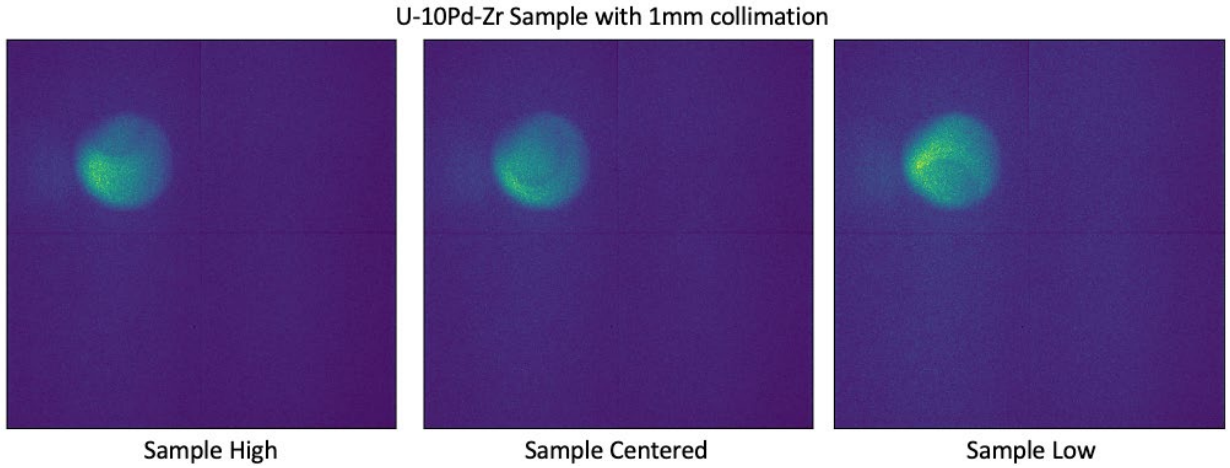

Figure 22. Summed image stacks, equivalent to a white beam source, from the MCP-Timepix detector in the FP5 cave of the three setups using the 1mm collimation. With this collimation, the U-10Zr-1Pd sample was vertically moved through the beam. This setup allowed for the NRTA measurements at the 60m SILO station to have a coarse spatial resolution.

The main idea behind illuminating only half the sample was specifically to see if there were any variations of isotopes observed in the NTRA spectra extracted from the 60 meter TRIPLE detector. Given that there is no spatial resolution with this detector and the 50 meter distance between sample and detector, we are able to create coarse spatially dependent NTRA spectra that would allow us to observe variations in lighter isotopes that have neutron absorption resonances that are too high in energy to see at the shorter flight path station (MCP-Timepix detector in the cave).

6.2.1 Initial Data and Pre-processing of FP5 Measurements

Experimentally, 2D transmission spectra can be obtained from taking the ratio of the neutron counts observed with the sample in the beam, C_{in}, to the neutron counts with the sample out of the beam, C_{out}. Taking into account the background and neutron exposure times, the 2D transmission spectra can be written as,

$$T_{exp}(E_n, x, y) = N_t \frac{C_{in}(E_n, x, y) - B_{in}(E_n, x, y)}{C_{out}(E_n, x, y) - B_{out}(E_n, x, y)}$$

Here, N_t is the normalization constant or scale factor between an image taken with the sample in and an image with the sample out (accounting for differences in count time or accelerator variations), $B_{in}(E_n,x,y)$ is the image background with the sample in, and $B_{out}(E_n,x,y)$ is the image background with the sample out. The far most right plot in Figure 23 illustrates what these neutron counts look like as a function of energy of the U-10Zr-1Pd sample ($C_{in} - B_{in}$) and open beam ($C_{out} - B_{out}$) after image normalization and averaged over a region of interest (x,y) that encompasses the sample, which is shown as a red circle in the two most left images in Figure 23. The resonances visible in the open beam data are from the tantalum plate and are used to estimate the background for the sample and open beam data. Upward spikes in the raw data are due to the Gd dopant in the MCPs. Both features disappear during the normalization process.

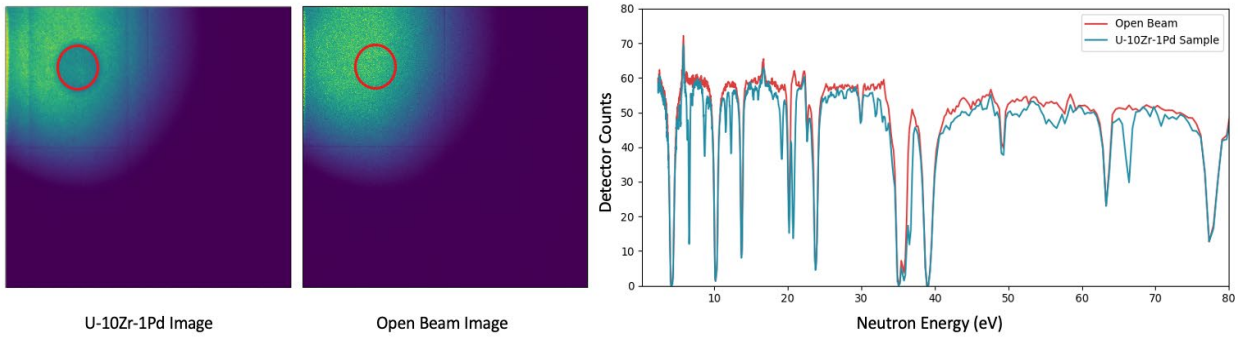

Figure 23. (Left) Raw summed image stacks of the U-10Zr-1Pd sample in the beam and out of the beam. The red circle indicates the region of interest for which average transmission spectra as a function of neutron energy are calculated. (Right) Average raw pixel counts within the region of interest for the U-10Zr-1Pd sample, along with the corresponding open beam spectra as a function of neutron energy. The resonances seen for the open beam spectrum are from the Ta calibration filter installed upstream in the neutron beam.

Ultimately, transmission spectra can be extracted for each pixel of our data set providing we have sufficient neutron statistics per such a small area (55x55 μm^2). Each of these transmissions will then be used to extract isotopic information as observed in the sample over that given pixel. Doing this over all pixels will then result in multiple 2D images that represent density maps of each isotope present. To obtain best possible per-pixel counting statistics and map isotopes with lower concentrations, such as fission products, much longer count times than available at the end of the 2019 LANSCE run cycle will be needed. These are available in the 2020 LANSCE run cycle.

Additionally, similar preprocessing for the data recorded with the TRIPLE detector is needed to generate a single transmission over the complete field of view. This pre-processing of the TRIPLE data is ongoing, though some raw data is shown in Figure 24. This detector, built in the 1990, was recently re-activated on FP5 after a hiatus of ~15 years. Data acquisition and data analysis with modern electronics and computer codes, respectively, are still under development.

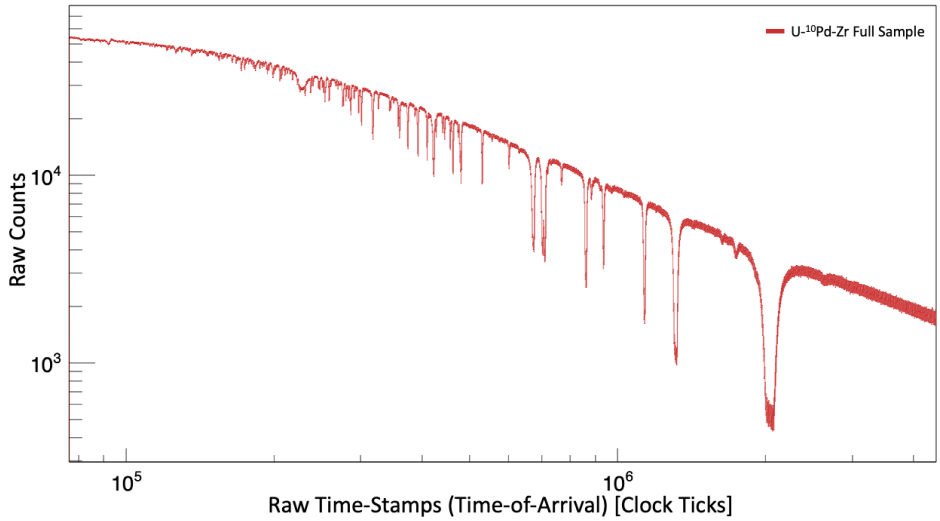

Figure 24. Raw data from the setup with the full sample illuminated by the neutron beam as recorded in the TRIPLE detector. This spectrum is the sum of all 55 detectors. Given the longer flight path, the neutron energy resolution is much better at higher neutron energies than what is observed in the FP5 cave at 9m source-detector distance with the MCP-Timepix detector. Furthermore, the 4 cm boron-doped liquid scintillator provides detection efficiencies of ~71% for 1keV neutron energies viz. negligible efficiency of the MCPs at these neutron energies.

6.2.2 Initial Transmission Data Analysis

Once a transmission spectrum as a function of neutron energy has been properly calculated from the given raw data, areal densities of specific isotopes can be extracted via the following equation,

$$\mathrm{T}_{\mathrm{exp}}(E_n, x, y) \;=\; \exp\left(\sum_k n_{k,x,y}\;\sigma_{k,tot}(E_n)\right)$$

Here, $\sigma_{k,tot}(E_n)$ is the broadened total neutron cross section as a function of incoming neutron energy, and n_k is the areal density in atoms per barn of the isotopes present in a given pixel of the sample.

For this particular work, there are two separate methods that are actively pursued in using the above equation to extract isotopic information. The first method utilizes a least square fitting of a theoretical estimate of the transmission to the one that is experimentally measured. This is mostly done with the R-matrix code SAMMY [79], which uses evaluated nuclear resonance data generated from ENDF [88]. This type of analysis is time consuming due to manual interactions with the code to identify proper starting values as well as fitting strategies, yet it is considered most accurate. The second method employs automatic background estimation using linear programming techniques as well as state-of-the-art machine learning algorithms along with ENDF evaluated neutron cross-sections to extract isotopic information. While less accurate, this method requires very little user interaction and is done in seconds. Both approaches are briefly described below.

6.2.2.1 Resonance fitting via SAMMY

Once transmission spectra have been created from the raw data, either from the TRIPLE or MCP-Timepix detector, isotopic areal densities can be extracted by fitting a theoretical estimate of the transmission function using the least square fitting method against the experimental data. This can be done using the code SAMMY, which uses an R-Matrix formalism to build a transmission function based on neutron resonances parameter data. Preliminary results of this type of analysis for data from the sample region, highlighted by the red circle in Figure 23, are shown in Figure 25. Clearly, three resonances at ~5 eV are

not properly included in the fit yet. To map the density of various isotopes accurately, this type of analysis has to be conducted for each pixel (or groups of pixels at a reduced resolution).

The top part of Figure 25 shows the experimental transmission data, along with the resulting SAMMY fit based on predefined set of resonances parameters as deposited in the ENDF database. For this SAMMY fit the included resonances were from ^{235}U, ^{238}U, and ^{108}Pd. Only resonances within the neutron energy range of 0.1-100 eV were used. The bottom part of Figure 25 shows the difference between the experimental and theoretically transmission spectra. This analysis is at a preliminary stage and several additional isotopes need to be included in the SAMMY analysis. It is worth pointing out that while cross-sections of e.g. uranium isotopes are well known and can be considered accurate, resonances of e.g. the Pd isotopes may be less well known. While for the uranium isotopes only the areal density is varied, for these resonances also parameters such as resonance energy or width may have to be varied, further complicating the analysis.

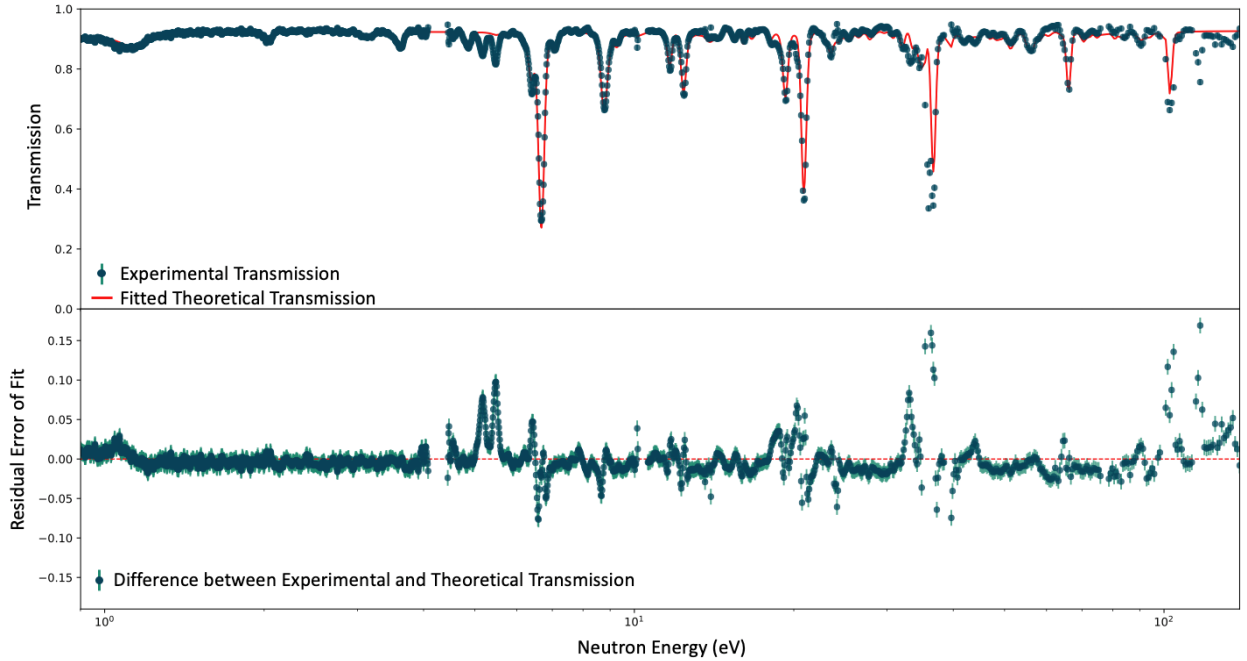

Figure 25. Initial fitting results from SAMMY on transmission spectra taken over the entire U-10Zr-1Pd sample. Fitting was done recursively until isotopic fit parameters converged. Three resonances around 5 eV still need to be identified and included in further SAMMY fits.

6.2.2.2 Isotope Density Estimation Based on Machine Learning

Funded by a LANL LDRD project on computational imaging, background estimation based on linear programming and isotope identification and density estimation via dictionary based machine learning (*B*asis *P*ursuit *De*N*o*ising, BPDN) are developed for energy-resolved neutron imaging at LANL. The data collected here is used as a test case for these algorithms with the goal to accelerate identification of isotopes present in the collected data as well as fast estimation of isotope densities. Since the latter can be done during the experiment, it may allow to identify regions of interest which are subsequently characterized during the same beam time, e.g. with a smaller collimator. Some preliminary results are shown here. Together with the algorithms, graphical output can be produced that allows quicker comparison of resonance profiles with experimental data to verify automated results manually. The code imports isotope cross-sections of user-defined candidates from the ENDF database.

This code is under development, with the current results included here to demonstrate progress towards accelerating the processing of energy-resolved neutron imaging data. It is unclear at this time if the machine learning algorithm will be able to replace a full SAMMY analysis or if they will become a tool to automate an accurate analysis with SAMMY based on approximation of areal densities. At this point, these results are by no mean quantitative or reliable. It is, however, worth pointing out that results like the isotope density maps in Figure 28 can be obtained within seconds from a list of candidate isotopes. On the other hand, isotope density maps with SAMMY require manual identification of isotopes, estimation of starting values for the fit, and repetition of the SAMMY fit for hundreds of pixels or pixel groups.

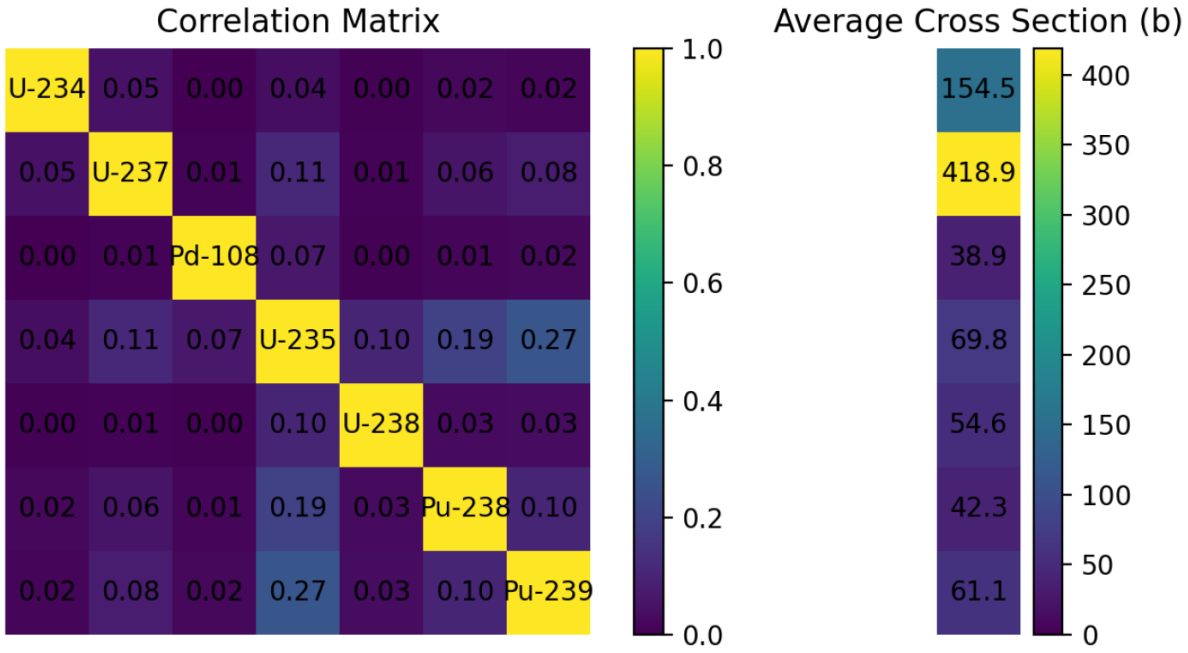

Figure 26: Weighted correlation matrix of isotope cross-sections included in the analysis. Bright yellow colors indicates a high correlation, i.e. isotopes are more likely to be confused during the processing, while dark blue colors indicate low correlation. The data on the right shows the cross-section averaged over the accessible energy range and weighed by the incident neutron flux.

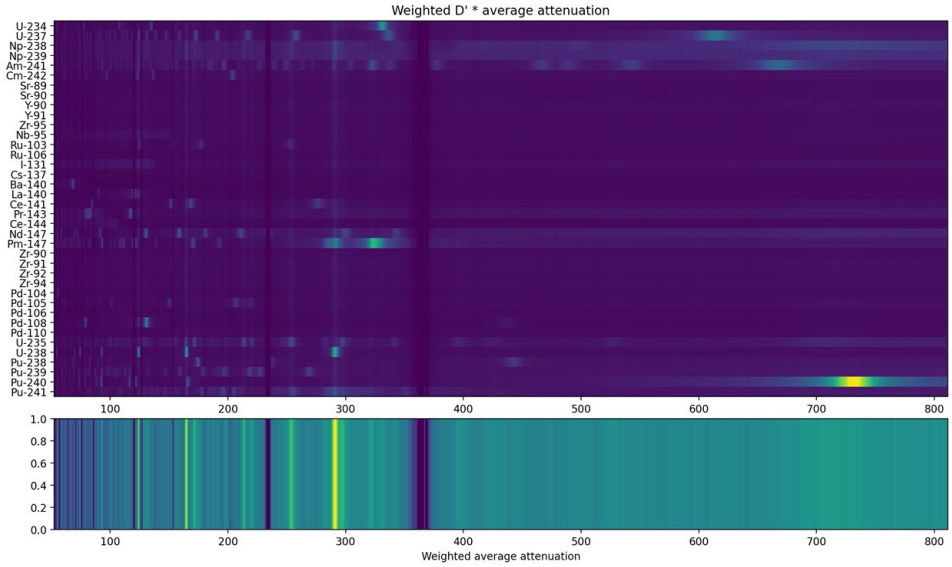

Figure 27: Graphical comparison of cross-sections of isotope candidates (top) with the experimental data (bottom). All data is displayed in time-of-flight channels.

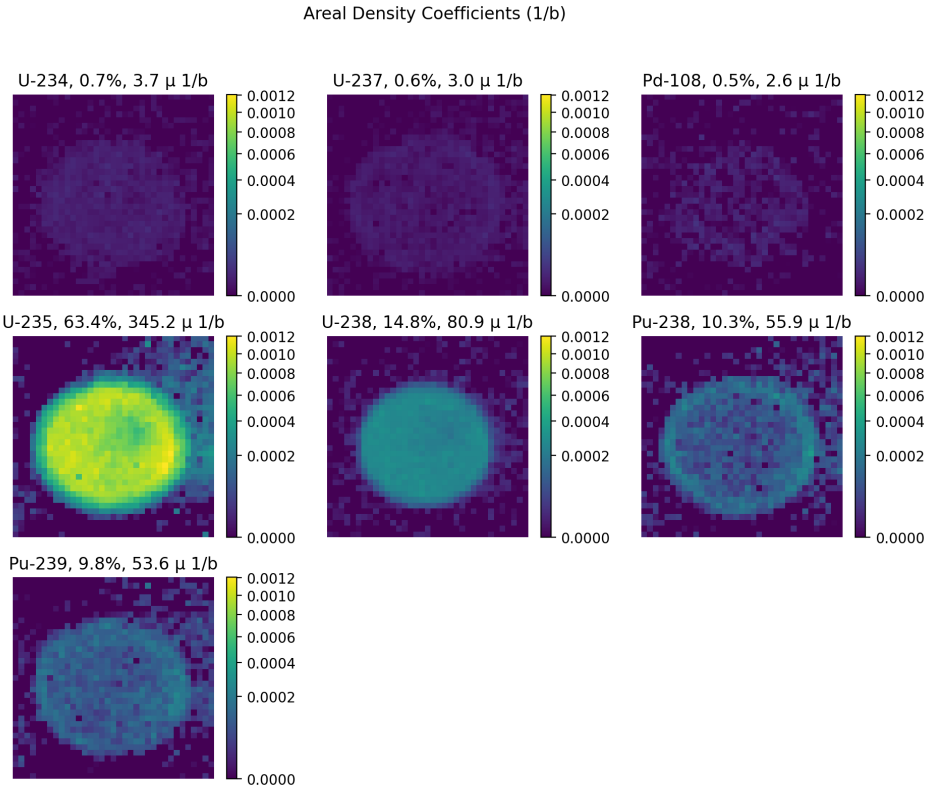

Figure 28: Preliminary maps of signal strengths from different isotopes resulting from a machine learning based mapping algorithm.

7. Conclusions & FY21 work

Pulsed neutron techniques provide substantial advantages over post-irradiation examination techniques presently available in proximity to the Advanced Test Reactor at INL. This was demonstrated at LANSCE for various fresh fuels (oxide, silicide, metallic etc.) and documented in previous reports [2,3,12,13,21,22]. In this report we demonstrated handling and preliminary pulsed neutron characterization of an irradiated sample emitting a dose rate of ~3R/hr on contact. The sample was received in late November of 2019 and within the remaining month in the 2019 LANSCE run cycle the preliminary data reported here were collected. For the 2020 LANSCE run cycle, the following measurements are planned:

- Energy-resolved neutron imaging and CT using the pixilated ^{10}B loaded MCP time-of-flight imaging detector described before. This will provide the 3D spatial distribution of isotopes from areal density measurements of isotopes from the resonances in the transmission signal. The CT measurement using this detector will provide average and spatially resolved isotope distributions as well as the basis for fiducials for the subsequent measurements. We expect this measurement to take 8 days of beam time.
- Neutron resonance transmission analysis (NRTA) using a 4cm thick, 80 cm diameter liquid scintillator detector with 55 photomultiplier tubes at the 60m station of FP5 will be conducted with the sample in the same location and the beam collimated to ~1mm. This will allow to map e.g. the concentration of Zr, Pd, potentially fission products or other isotopes with resonance not within the energy range of the imaging detector. We expect this measurement to take ~24 hours per sample location. For 12 locations to scan the sample in 1mm increments vertically and horizontally we expect 12 days of beam time.
- Time-of-flight neutron diffraction on the HIPPO diffractometer in principle allows phase identification, determination of weight fractions of the phases, and texture measurements for phases >~0.5 wt.%. Some information of grain sizes, microstrain and dislocation densities can be also determined. However, the high enrichment of this sample leads to strong absorption of thermal neutrons and the measurements may be limited to bulk characterization of the phase composition and texture. We expect ~24 hours of beamtime per sample rotation and therefore 3 days on HIPPO for the three rotations.
- High resolution powder diffraction on the SMARTS instrument, using a 2x2mm^2 collimated beam will verify the phase identification conducted on HIPPO with a higher spatial resolution. The sample will be moved by the SMARTS translator table to probe different volumes. We expect this measurement to take 48 hours per data point, therefore 12 days to scan 6 data points.

8. Acknowledgements

This work was funded by the Fuel Cycle R&D program overviewed by Steve Hayes (INL) and Kenneth J. McClellan (LANL). Darrin Byler (LANL) is the responsible work package manager. We appreciate an NSUF grant to conduct more extensive measurements in the upcoming 2020 LANSCE run cycle. The work to develop advanced analysis techniques for energy-resolved imaging was funded by LDRD-DR 20200061DR, “Prioritizing the Prior: Advanced Inversion Algorithms for Scientific Data Analysis”, PI Brendt Wohlberg, Co-PIs Cristina Garcia-Cordona and Sven Vogel. Support for the visit of Charlie Bouman and Thilo Balke to LANL in July 2019 to start this effort by a rapid response grant from LANL’s Institute for Materials Science is gratefully acknowledged.

9. References

[1] McClellan, K., Chichester, H., Hayes, S., & Voit, S. (2013). Summary of the minor actinide-bearing MOX AFC-2C and-2D irradiations, Proceedings of FR13: International Conference on

Fast Reactors and Related Fuel Cycles: Safe Technologies and Sustainable Scenarios, March 4-7, 2013, Paris, France.

[2] Vogel et al., “Assessment of advanced NDE techniques and the path forward to evaluating an AFC-2 irradiated fuel pin”, LA-UR 13-2167.

[3] Sven C. Vogel, Adrian S. Losko, Reeju Pokharel, Timothy L Ickes, James Hunter, Donald W. Brown, Stewart L. Voit, Anton S. Tremsin, Mark A.M. Bourke, Kenneth J. McClellan, “Non-destructive Pre-irradiation Assessment of UN / U-Si “LANL1” ATF formulation”, Report to DOE/NE, LA-UR-16-27110 (2016).

[4] Vogel, S. C. (2013). A review of neutron scattering applications to nuclear materials. ISRN Materials Science, 2013.

[5] M. B. Aufderheide III, H.-S. Park, E. P. Hartouni, P. D. Barnes, D. M. Wright, R. M. Bionta, J. D. Zumbro, C. L. Morris, “Proton radiography as a means of material characterization”, AIP Conference Proceedings, 497 (1999) 706.

[6] C. Morris, M. Bourke, D. Byler, C. Chen, G. Hogan, J. Hunter, K. Kwiatkowski, F. Mariam, K. McClellan, F. Merrill, et al., “Qualitative comparison of bremsstrahlung X-rays and 800 MeV protons for tomography of urania fuel pellets”, Review of Scientific Instruments 84 (2013) 023902.

[7] Lisowski, P. W., & Schoenberg, K. F. (2006). The Los Alamos neutron science center. Nuclear Instruments and Methods in Physics Research Section A: Accelerators, Spectrometers, Detectors and Associated Equipment, 562(2), 910-914.

[8] M.D. Roth et al. "Bright laser-driven neutron source based on the relativistic transparency of solids." Physical review letters 110, no. 4 (2013): 044802.

[9] Fernández, J. C., Cort Gautier, D., Huang, C., Palaniyappan, S., Albright, B. J., Bang, W., ... & Roth, M. (2017). Laser-plasmas in the relativistic-transparency regime: Science and applications. Physics of Plasmas, 24(5), 056702.

[10] M. Roth, S. C. Vogel, M. A. M. Bourke, J. Fernandez, M. Mocko, S. Glenzer, W. Leemans, C.W. Siders, C. Haefner, “Assessment of Laser-Driven Pulsed Neutron Sources for Poolside Neutron-based Advanced NDE – A Pathway to LANSCE-like Characterization at INL”, Report NTRD-FUEL-2017-000064 to DOE/NE, LA-UR-17-23190 (2017).

[11] Vogel, S. C., Bourke, M. A., & Losko, A. S. (2016). Neutron based evaluation in support of NEAMS (No. LA-UR--16-23977). Los Alamos National Lab.(LANL), Los Alamos, NM (United States).

[12] Vogel, S.C., Borges, N.P., Losko, A.S., Mosby, S.M., Voit, S.L., White, J.T., Byler, D.D., Dunwoody, J.T., Nelson, A.T. and Mcclellan, K.J., 2017. Neutron Characterization of Encapsulated ATF-1/LANL-1 Mockup Fuel Capsules (No. LA-UR-17-28837). Los Alamos National Lab.(LANL), Los Alamos, NM (United States).

[13] Vogel, S. C., Losko, A. S., Bourke, M. A. M. , McClellan, K. J., Fielding, R. (2017) Neutron Characterization of Encapsulated Metallic Fuel, Los Alamos National Lab.(LANL), Los Alamos, NM (United States).

[14] Brown, D. W., Okuniewski, M. A., Almer, J. D., Balogh, L., Clausen, B., Okasinski, J. S., & Rabin, B. H. (2013). High energy X-ray diffraction measurement of residual stresses in a monolithic aluminum clad uranium–10wt% molybdenum fuel plate assembly. Journal of Nuclear Materials, 441(1), 252-261.

[15] Eggl, E., Dierolf, M., Achterhold, K., Jud, C., Günther, B., Braig, E., Gleich, B. and Pfeiffer, F., 2016. The Munich compact light source: initial performance measures. Journal of synchrotron radiation, 23(5), pp.1137-1142.

[16] A. Tremsin, S. Vogel, M. Mocko, M. Bourke, V. Yuan, R. Nelson, D. Brown, B. Feller, "Non-destructive studies of fuel rodlets by neutron resonance absorption radiography and thermal neutron radiography", Journal of Nuclear Materials, 440 (2013) 633–646.

[17] Tremsin, A. S., Losko, A. S., Vogel, S. C., Byler, D. D., McClellan, K. J., Bourke, M. A. M., & Vallerga, J. V. (2017). Non-contact measurement of partial gas pressure and distribution of elemental composition using energy-resolved neutron imaging. AIP Advances, 7(1), 015315.

[18] Huang, J., Vogel, S. C., Poole, W. J., Militzer, M., & Jacques, P. (2007). The study of low-temperature austenite decomposition in a Fe–C–Mn–Si steel using the neutron Bragg edge transmission technique. Acta materialia, 55(8), 2683-2693.

[19] Woracek, R., Santisteban, J., Fedrigo, A., & Strobl, M. (2018). Diffraction in neutron imaging—A review. Nuclear Instruments and Methods in Physics Research Section A: Accelerators, Spectrometers, Detectors and Associated Equipment, 878, 141-158.

[20] AS Tremsin, JB McPhate, JV Vallerga, OHW Siegmund, JS Hull, WB Feller, and E Lehmann. High-resolution neutron radiography with microchannel plates: Proof-of-principle experiments at psi. Nuclear Instruments and Methods in Physics Research Section A: Accelerators, Spectrometers, Detectors and Associated Equipment, 605(1):103–106, 2009.

[21] Vogel, S. C., Byler, D. D., Kardoulaki, E., Losko, A. S., Mcclellan, K. J., Tremsin, A., ... & White, J. T. (2018). Neutron Resonance Spectroscopy Applications for Nuclear Fuel Characterization (No. LA-UR-18-24874). Los Alamos National Lab.(LANL), Los Alamos, NM (United States).

[22] Bourke, M. A., Vogel, S. C., Voit, S. L., Mcclellan, K. J., Losko, A. S., & Tremsin, A. (2016). Non destructive examination of UN/U-Si fuel pellets using neutrons (preliminary assessment) (No. LA-UR--16-22179). Los Alamos National Lab.(LANL), Los Alamos, NM (United States).

[23] Jenssen, H. K., Oberländer, B. C., Beenhouwer, J. D., Sijbers, J., & Verwerft, M. (2014). Neutron radiography and tomography applied to fuel degradation during ramp tests and loss of coolant accident tests in a research reactor. Progress in Nuclear Energy, 72, 55-62.

[24] Lehmann, E. H., Vontobel, P., & Hermann, A. (2003). Non-destructive analysis of nuclear fuel by means of thermal and cold neutrons. Nuclear Instruments and Methods in Physics Research Section A: Accelerators, Spectrometers, Detectors and Associated Equipment, 515(3), 745-759.

[25] Wei, G., Han, S., Wang, H., Hao, L., Wu, M., He, L., ... & Chen, D. (2013). Design of the testing set-up for a nuclear fuel rod by neutron radiography at CARR. Physics Procedia, 43, 307-313.

[26] Chaudhary, U. K., Iqbal, M., & Ahmad, M. (2010). Defect sizing of post-irradiated nuclear fuels using grayscale thresholding in their radiographic images. Nuclear Engineering and Design, 240(10), 3455-3461.

[27] Nazemi, E., Rokrok, B., Movafeghi, A., Dastjerdi, M. C., & Dinca, M. (2019). Obtaining optimum exposure conditions for digital X-ray radiography of fresh nuclear fuel rods. Nuclear Instruments and Methods in Physics Research Section A: Accelerators, Spectrometers, Detectors and Associated Equipment, 923, 88-96.

[28] Sim, C. M., Kim, T., Oh, H. S., & Kim, J. C. (2013). Measurement of ballooning gap size of irradiated fuels using neutron radiography transfer method and HV image filter. Journal of the Korean Society for Nondestructive Testing, 33(2), 212-218.

[29] De Beer, F. C. (2015). Neutron-and X-ray radiography/tomography: Non-destructive analytical tools for the characterization of nuclear materials. Journal of the Southern African Institute of Mining and Metallurgy, 115(10), 913-924.

[30] Singh, J. L., Mondal, N., Dhotre, M., Pandit, K., Bhandekar, A., Kumawat, N., ... & Anantharaman, S. (2011). Non-destructive evaluation of irradiated nuclear fuel pins at Cirus Research Reactor by neutron radiography. In National Seminar & Exhibition on Non-Destructive Evaluation (pp. 11-15).

[31] Parker, H. M. D., & Joyce, M. J. (2015). The use of ionising radiation to image nuclear fuel: A review. Progress in Nuclear Energy, 85, 297-318.

[32] Birtcher, R. C., Mueller, M. H., Richardson, J. W., & Faber, J. (1989). Neutron irradiated uranium silicides studied by neutron diffraction and Rietveld analysis. MRS Online Proceedings Library Archive, 166.

[33] Birtcher, R. C., Richardson, J. W., & Mueller, M. H. (1994). Neutron Diffraction Study of Radiation Damage in U 3 Si at 30° C and 350° C. MRS Online Proceedings Library Archive, 373.

[34] Birtcher, R. C., Richardson, J. W., & Mueller, M. H. Amorphization of U_3Si_2 by ion or neutron irradiation, J. Nucl. Materials, 230, 158-163 (1996).

[35] Birtcher, R. C. (1997). Neutron irradiation effect studies at IPNS. Neutron News, 8(3), 8-11.

[36] Richardson Jr, J. W., Birtcher, R. C., & Chan, S. K. (1997). Neutron irradiation induced amorphization of uranium silicides. Physica B: Condensed Matter, 241, 390-392.

[37] Rietveld, H. (1969). A profile refinement method for nuclear and magnetic structures. Journal of applied Crystallography, 2(2), 65-71.

[38] Conlon, K. T., & Sears, D. F. (2006). Neutron powder diffraction of irradiated low-enriched uranium-molybdenum dispersion fuel. In: Proceedings of 10th International Topical Meeting on Research Reactor Fuel Management, 30 April - 3 May 2006, Sofia, Bulgaria, p. 104-108.

[39] Conlon, K., & Sears, D. (2007). Neutron powder diffraction of U-Mo fuel irradiated to 60 atom% 235 U burnup. In: Proceedings of 11th International Topical Meeting on Research Reactor Fuel Management (RRFM) and meeting of the International Group on Reactor Research (IGORR); Lyon (France); 11-15 Mar 2007, p. 140-144.

[40] Sears, D., Wang, N., Rogge, R., Swainson, I., & Donaberger, R. (2011). Neutron Diffraction Analysis of High Burnup LEU Fuel from NRU. Available online at http://cins.ca/docs/exp_rep/CNBC-2011-MS-5.pdf

[41] Schillebeeckx, P., Becker, B., Harada, H., Kopecky, S. (2014) Neutron Resonance Spectroscopy for the Characterization of Materials and Objects, JRC Science and Policy Reports, Report EUR26848EN.

[42] Schillebeeckx, P., Becker, B., Danon, Y., Guber, K., Harada, H., Heyse, J., Junghans, A.R., Kopecky, S., Massimi, C., Moxon, M.C. and Otuka, N., 2012. Determination of resonance parameters and their covariances from neutron induced reaction cross section data. Nuclear Data Sheets, 113(12), pp.3054-3100.

[43] Sterbentz, J. W., & Chichester, D. L. (2010). Neutron resonance transmission analysis (NRTA): a nondestructive assay technique for the next generation safeguards initiative's plutonium assay challenge (No. INL/EXT-10-20620). Idaho National Laboratory (INL).

[44] Chichester, D. L., & Sterbentz, J. W. (2011, July). A second look at neutron resonance transmission analysis as a spent fuel NDA technique. In Conference: INMM 52nd Annual

Meeting, Palm Desert, CA USA,< http://www. inl. gov/technicalpublications/Documents/4953376. pdf.

[45] Chichester, D. L., & Sterbentz, J. W. (2011). Neutron resonance transmission analysis (NRTA): initial studies of a method for assaying plutonium in spent fuel (No. INL/CON-10-20684). Idaho National Laboratory (INL).

[46] Harada, H., Kitatani, F., Koizumi, M., Takamine, J., Kureta, M., Tsutiya, H., Iimura, H., Seya, M., Becker, B., Kopecky, S. and Schillebeeckx, P., 2014. Neutron resonance densitometry for particle-like debris of melted fuel. Nuclear Data Sheets, 118, pp.502-504.

[47] Heyse, J., Becker, B., Harada, H., Kitatani, F., Koizumi, M., Kopecky, S., ... & Tsuchiya, H. (2015, April). Characterization of melted fuel by neutron resonance spectroscopy. In 2015 4th International Conference on Advancements in Nuclear Instrumentation Measurement Methods and their Applications (ANIMMA) (pp. 1-6). IEEE.

[48] Toh, Y., Ebihara, M., Kimura, A., Nakamura, S., Harada, H., Hara, K.Y., Koizumi, M., Kitatani, F. and Furutaka, K., 2014. Synergistic effect of combining two nondestructive analytical methods for multielemental analysis. Analytical chemistry, 86(24), pp.12030-12036.

[49] Priesmeyer, H. G., & Harz, U. (1975). Isotopic content determination in irradiated fuel by neutron transmission analysis. Atomkernenergie, 25(2), 109-113.

[50] Priesmeyer, H. G., & Harz, U. (1976). Isotopic assay in irradiated fuel by neutron resonance analysis. Safeguarding nuclear materials, 20-24.

[51] Priesmeyer, H. G., Harz, U. & Fischer, P. (1981), Neutron Physics Activities at the FRG-1 Research Reactor, IAEA Seminar on Research Reactor Operation, Jülich, Germany, September 14-18, 1981, IAEA-SR-77/67.

[52] Behrens, J. W., Johnson, R. G., & Schrack, R. A. (1984). Neutron resonance transmission analysis of reactor fuel samples. Nuclear technology, 67(1), 162-168.

[53] Bowman, C. D., Schrack, R. A., Behrens, J. W., & Johnson, R. G. (1983). Neutron resonance transmission analysis of reactor spent fuel assemblies. In Neutron Radiography (pp. 503-511). Springer, Dordrecht.

[54] Tamaki, M., Iida, K., Mori, N., Lehmann, E. H., Vontobel, P., & Estermann, M. (2005). Dy-IP characterization and its application for experimental neutron radiography tests under realistic conditions. Nuclear Instruments and Methods in Physics Research Section A: Accelerators, Spectrometers, Detectors and Associated Equipment, 542(1-3), 320-323.

[55] Degueldre, C., Bertsch, J., & Martin, M. (2016). Post irradiation examination of nuclear fuel: Toward a complete analysis. Progress in Nuclear Energy, 92, 242-253.

[56] Groeschel, F., Schleuniger, P., Hermann, A., Lehmann, E., & Wiezel, L. (1999). Neutron radiography of irradiated fuel rod segments at the SINQ: loading, transfer and irradiation concept. Nuclear Instruments and Methods in Physics Research Section A: Accelerators, Spectrometers, Detectors and Associated Equipment, 424(1), 215-220.

[57] Vontobel, P., Tamaki, M., Mori, N., Ashida, T., Zanini, L., Lehmann, E. H., & Jaggi, M. (2006). Post-irradiation analysis of SINQ target rods by thermal neutron radiography. Journal of nuclear materials, 356(1-3), 162-167.

[58] Lehmann, E. H., Vontobel, P., & Wiezel, L. (2001). The investigation of highly activated samples by neutron radiography at the spallation source SINQ. Nondestructive Testing and Evaluation, 16(2-6), 203-214.

[59] Post Irradiation Examination Guide, Idaho National Laboratory report INL/MIS-15-35828 (2015).

[60] Porter, D. L., & Tsai, H. (2012). Full-length U–xPu–10Zr (x= 0, 8, 19 wt.%) fast reactor fuel test in FFTF. Journal of Nuclear Materials, 427(1-3), 46-57.

[61] Teague, M., Gorman, B., King, J., Porter, D., & Hayes, S. (2013). Microstructural characterization of high burn-up mixed oxide fast reactor fuel. Journal of Nuclear Materials, 441(1-3), 267-273.

[62] Harp, J. M., Capriotti, L., & Chichester, H. J. (2019). Postirradiation Examination of FUTURIX-FTA metallic alloy experiments. Journal of Nuclear Materials, 515, 420-433.

[63] Rice, F., Williams, W., Robinson, A., Harp, J., Meyer, M., & Rabin, B. (2015). RERTR-12 Post-irradiation examination summary report (No. INL/EXT-14-33066). Idaho National Lab.(INL), Idaho Falls, ID (United States).

[64] Craft, A. E., Wachs, D. M., Okuniewski, M. A., Chichester, D. L., Williams, W. J., Papaioannou, G. C., & Smolinski, A. T. (2015). Neutron radiography of irradiated nuclear fuel at Idaho National Laboratory. Physics Procedia, 69, 483-490.

[65] Craft, A. E., Papaioannou, G. C., Chichester, D. L., & Williams, W. J. (2017). Conversion from film to image plates for transfer method neutron radiography of nuclear fuel. Physics Procedia, 88, 81-88.

[66] Craft, A. E., & Barton, J. P. (2017). Applications of neutron radiography for the nuclear power industry. Physics Procedia, 88, 73-80.

[67] DOE Standard “Preparation of Nonreactor Nuclear Facility Documented Safety Analysis”, DOE-STD-3009-2014, November 2014.

[68] Accelerator Facility Safety Implementation Guide for DOE O 420.2C, Safety of Accelerator Facilities, US Department of Energy, Office of Science, DOE G 420.2-1A, August 1, 2014.

[69] Wenk, H. R., Lutterotti, L., & Vogel, S. (2003). Texture analysis with the new HIPPO TOF diffractometer. Nuclear Instruments and Methods in Physics Research Section A: Accelerators, Spectrometers, Detectors and Associated Equipment, 515(3), 575-588.

[70] Vogel, S. C., Hartig, C., Lutterotti, L., Von Dreele, R. B., Wenk, H. R., & Williams, D. J. (2004). Texture measurements using the new neutron diffractometer HIPPO and their analysis using the Rietveld method. Powder Diffraction, 19(1), 65-68.

[71] Takajo, S., & Vogel, S. C. (2018). Determination of pole figure coverage for texture measurements with neutron time-of-flight diffractometers. Journal of Applied Crystallography, 51(3), 895-900.

[72] Losko, A. S., Vogel, S. C., Reiche, H. M., & Nakotte, H. (2014). A six-axis robotic sample changer for high-throughput neutron powder diffraction and texture measurements. Journal of Applied Crystallography, 47(6), 2109-2112.

[73] Mocko, M., Muhrer, G. and Tovesson, F., 2008. Advantages and limitations of nuclear physics experiments at an ISIS-class spallation neutron source. Nuclear Instruments and Methods in Physics Research Section A: Accelerators, Spectrometers, Detectors and Associated Equipment, 589(3), pp.455-464.

[74] Mocko, M., & Muhrer, G. (2013). Fourth-generation spallation neutron target-moderator-reflector-shield assembly at the Manuel Lujan Jr. neutron scattering center. Nuclear Instruments and Methods in Physics Research Section A: Accelerators, Spectrometers, Detectors and Associated Equipment, 704, 27-35.

[75] Tremsin, A. S., McPhate, J. B., Vallerga, J. V., Siegmund, O. H. W., Feller, W. B., Lehmann, E., & Dawson, M. (2011). Improved efficiency of high resolution thermal and cold neutron imaging. Nuclear Instruments and Methods in Physics Research Section A: Accelerators, Spectrometers, Detectors and Associated Equipment, 628(1), 415-418.

[76] Tremsin, A. S., McPhate, J. B., Vallerga, J. V., Siegmund, O. H. W., Feller, W. B., Lehmann, E., ... & Dawson, M. (2011). High-resolution neutron microtomography with noiseless neutron counting detector. Nuclear Instruments and Methods in Physics Research Section A: Accelerators, Spectrometers, Detectors and Associated Equipment, 652(1), 400-403.

[77] Tremsin, A.S., Kockelmann, W., Pooley, D.E. and Feller, W.B., 2015. Spatially resolved remote measurement of temperature by neutron resonance absorption. Nuclear Instruments and Methods in Physics Research Section A: Accelerators, Spectrometers, Detectors and Associated Equipment, 803, pp.15-23.

[78] http://web.ornl.gov/sci/nuclear_science_technology/nuclear_data/sammy/

[79] N. Larson, "Updated user's guide for SAMMY: multilevel R-matrix fits to neutron data using Baye's equations." No. ORNL/TM-9179. Oak Ridge National Lab., TN (USA), 1984.

[80] M.C. Moxon, T.C. Ware, C.J. Dean, REFIT-2009 A Least-Square Fitting Program for Resonance Analysis of Neutron Transmission. Capture, Fission and Scattering Data Users' Guide for REFIT-2009-10 (UKNSFP243, 2010).

[81] MessaoudiI, C., Boudier, T., Sorzano, C. O. S., & Marco, S. (2007). TomoJ: tomography software for three-dimensional reconstruction in transmission electron microscopy. BMC bioinformatics, 8(1), 288.

[82] Tremsin, A. S., Craft, A. E., Bourke, M. A. M., Smolinski, A. T., Papaioannou, G. C., Ruddell, M. A., ... & Tedesco, J. (2018). Digital neutron and gamma-ray radiography in high radiation environments with an MCP/Timepix detector. Nuclear Instruments and Methods in Physics Research Section A: Accelerators, Spectrometers, Detectors and Associated Equipment, 902, 110-116.

[83] Tremsin, A. S., Craft, A. E., Papaioannou, G. C., Smolinski, A. T., Boulton, N. M., Ruddell, M. A., ... & Riley, K. D. (2019). On the possibility to investigate irradiated fuel pins non-destructively by digital neutron radiography with a neutron-sensitive microchannel plate detector with Timepix readout. Nuclear Instruments and Methods in Physics Research Section A: Accelerators, Spectrometers, Detectors and Associated Equipment, 927, 109-118.

[84] Yen, Y.F., Bowman, J.D., Bolton, R.D., Crawford, B.E., Delheij, P.P.J., Hart, G.W., Haseyama, T., Frankle, C.M., Iinuma, M., Knudson, J.N. and Masaike, A., 2000. A high-rate 10B-loaded liquid scintillation detector for parity-violation studies in neutron resonances. Nuclear Instruments and Methods in Physics Research Section A: Accelerators, Spectrometers, Detectors and Associated Equipment, 447(3), pp.476-489.

[85] Williams, W.J., Okuniewski, M.A., Vogel, S.C. and Zhang, J., 2020. In Situ Neutron Diffraction Study of Crystallographic Evolution and Thermal Expansion Coefficients in U-22.5 at.% Zr During Annealing. JOM, pp.1-9.

[86] Janney, D. E., & Papesch, C. A. (2015). FCRD Transmutation Fuels Handbook 2015 (No. INL/EXT--15-36520). Idaho National Laboratory (INL), Idaho Falls, ID (United States).

[87] Janney, D.E. and Hayes, S.L., 2018. Experimentally known properties of U-10Zr alloys: A critical review. Nuclear Technology, 203(2), pp.109-128.

[88] Brown, D.A., Chadwick, M.B., Capote, R., Kahler, A.C., Trkov, A., Herman, M.W., Sonzogni, A.A., Danon, Y., Carlson, A.D., Dunn, M. and Smith, D.L., 2018. ENDF/B-VIII. 0: The 8th

major release of the nuclear reaction data library with CIELO-project cross sections, new standards and thermal scattering data. Nuclear Data Sheets, 148, pp.1-142.